ABSTRACT

Title of Dissertation: SYNTHESIS AND CHARACTERIZATION OF DIBLOCK COPOLYMER TEMPLATED IRON OXIDE NANOPARTICLES

Pınar Akçora, Doctor of Philosophy, 2005

Dissertation directed by: Professor Peter Kofinas
Department of Chemical and Biomolecular Engineering

Templating ordered assemblies of magnetic oxide nanoparticles within self-assembled diblock copolymers of varying morphologies is an important problem with a wide applicability such as in electromagnetics, optical devices, metal catalysts, medicine and biology. In this thesis, the effects of different polymer structures on particle ordering and resultant magnetic properties have been investigated using various microstructure and magnetic characterization tools.

Ring-opening metathesis polymerization (ROMP) of norbornene and functionalized norbornene monomers has been used to synthesize diblock copolymers of narrow polydispersities using Grubbs' catalyst. These block copolymers can be used as templates to form inorganic nanoparticles. In this research, the structural and physical understanding of the inorganic-copolymer system was studied by

small-angle neutron and x-ray scattering techniques and transmission electron microscopy. Synthesis of γ-Fe_2O_3 nanoparticles has been achieved within novel block copolymers of (norbornene)-b-(deuterated norbornene dicarboxylic) acid and (norbornene methanol)-(norbornene dicarboxylic acid). The polymer morphologies were controlled by varying the volume fractions of the constituent blocks. The pure norbornene based diblock copolymer morphologies were demonstrated by electron microscopy for the first time. Spherical, cylindrical and lamellar morphologies of these novel diblock copolymers were reported. The block ratios of the synthesized polymers were determined using gel permeation chromatography - light scattering, elemental analysis and UV-VIS spectroscopy. Solution phase doping and submersion of thin films in metal salt solutions were employed as metal doping methods and the observed nanoparticle structures were compared to those of the undoped copolymer morphologies. This project reports on the types of templating structures and dispersion of the nanoparticles. The effects of particle interactions on the microphase separation and magnetic properties were also investigated. The knowledge gained from understanding the templating mechanism in block copolymer / iron oxide nanocomposites can be applied to other similar systems for a variety of biological and catalyst applications.

SYNTHESIS AND CHARACTERIZATION OF DIBLOCK COPOLYMER TEMPLATED IRON OXIDE NANOPARTICLES

by

Pınar Akçora

Dissertation submitted to the Faculty of the Graduate School of the
University of Maryland at College Park in partial fulfillment
of the requirements for the degree of
Doctor of Philosophy
2005

Advisory Committee:

Professor Peter Kofinas, Chairman/Advisor
Professor Robert M. Briber, Co-advisor
Professor Sheryl H. Ehrman
Professor Srinivasa R. Raghavan
Professor Panagiotis Dimitrakopoulos

DEDICATION

To the memory of my grandmother, Semiha Ayşe Yürekli.

ACKNOWLEDGEMENTS

I would like to thank my advisor, Prof. Peter Kofinas, for his support and encouragement during my research. He always believed in me and supported me at my difficult times. I am also very fortunate to work with Prof. Robert M. Briber as my co-advisor. He was always very helpful and available in his busy schedule to answer my questions. I would also like to thank Prof. Ehrman, Prof. Raghavan and Prof. Dimitrakopoulos for accepting to be in my thesis committee. From the first moment I mentioned my decision to pursue PhD degree, my family has always supported and encouraged me. I thank them for all their thoughts and support. Last, my thanks go to my dearest friend Ozgur. I would not be able to complete my PhD without his support and patience.

TABLE OF CONTENTS

LIST OF TABLES

LIST OF FIGURES

Chapter 1

Introduction

Magnetic nanoparticles are a subject of extensive research due to their unique magnetic properties and potential technological applications such as ferrofluids, recording tapes, ultra-high density data storage media, biomedical materials and catalysts.[1,2] Stabilization of nanoparticles to avoid interparticle aggregation and control of their spatial distribution and size within template materials are important factors in the design of nanoparticle synthesis and devices.[3,4] Block copolymers which microphase separate into ordered morphologies such as lamellar, cylindrical and spherical microdomains provide a self-assembled template for the synthesis of nanocomposites. These microdomains serve as nanoreactors within which a variety of nanoparticles can be synthesized.

The aim of this research was to synthesize magnetic nanoparticles in novel diblock copolymer systems and to investigate their structural and magnetic properties within different polymer structures. High-density magnetic particle arrays have been fabricated using several lithographic techniques including X-ray lithography and nanoimprint nanolithography.[5] Block copolymers provide a self-assembled

nanotemplate that can also be used for lithography.[6] Polymer nanotemplates can be used to produce ordered metal and metal oxide particles at room temperature. Fabrication of high density nanoparticles within controlled nanopatterns with improved catalytic, magnetic, optical and electromagnetic properties and exploring their structure-property relationship is the main objective of many research endeavors. The effect of different morphologies on the formation of metal oxide nanoparticles and their resultant properties will determine the fabrication and design of nanodevices for the above mentioned specific applications.

The synthesis of metal nanoparticles within the nanoscale morphologies of ordered block copolymers has been studied extensively by various techniques. One method is to attach a metal group as a pendant group to organometallic monomers. This method gives uniform dispersion of the metal precursor within the metal-containing block of the copolymer. PbS, CdS, ZnS, Ag and Pd clusters were synthesized with this method by R. E. Cohen's group at MIT.[7–12]

Metal atoms were deposited into liquid monomers such as liquid styrene and methyl methacrylate. In addition, deposition of metal atoms into polymers and styrene vapor was employed.[13] The incorporation of metal salts onto polymer films from supercritical CO_2, followed by reduction of salts to metal nanoclusters by chemical post-treatment has also been reported.[14]

One of the method used in the synthesis of nanoparticles is the nanoreactor scheme in which metals are incorporated into acid-containing domains of diblock copolymers from aqueous solution. In this method, metal ions diffuse into the hydrophilic domains of the polymer film. The loading is modified by pretreating the

polymer with aqueous sodium hydroxide. Protonated carboxylic acid groups are converted into sodium carboxylate in order to enhance the metal ion uptake by Na^+ cations. It has been observed that the rate and the equilibrium amount of metal ion increased after NaOH treatment.[15,16] This method produces successful doping in polymer films ranging in thickness from 10μ to 0.5mm. For microtomed films, very low metal salt concentrations were used (0.1M and 0.005M) to prevent formation of metal salt crystals on the film surface.

Metal doping from solution has been successful in amphiphilic polymers due to their high affinity to transition metal ions.[17] In previous studies, block copolymers containing carboxylic acid-functionalized blocks were synthesized and various metal clusters were incorporated into acid-containing domains by mixing polymers with metal salts in solution.[18,19] This technique is also based on the substitution of the carboxylic protons with the cations of the desired metal species. This method has the advantage of loading the sample in solution phase so that the metal ions are incorporated homogenously and the bulk films consist of well-dispersed nanoparticles. This loading method was used in this project. The mechanism of metal loading and its effect on the resultant nanocomposite morphology were examined and compared to the method where a pre-formed film is immersed in aqueous solution.

Another method developed in Cohen's group is the vapor permeation of metal alkyl compounds such as diethylzinc and dimethylcadmium into the polymer matrix.[20,21] Synthesis of PbS clusters within methyltetracyclododecene/norbornene dicarboxylic acid diblock copolymer was reported by Kane et al. Tetraethyl lead was coordinated with the carboxylate group on the block copolymer and then lead

was reduced to its divalent form by heat treatment and after reacting with H_2S, PbS nanoclusters were created.[22,23] Another method was the reduction of metal ions in ordered nanophases in concentrated block copolymer solutions.[24]

Wiesner et al. has synthesized block copolymer - ceramic hybrid materials with γ-Fe_2O_3 particles.[25,26] They have used diblock copolymers as structure directing agents. Aluminasilicate sol was mixed with a polymer solution and iron oxide particles in the sol-gel aluminasilicate synthesis. Phase behavior of these systems is similar to that of the systems where the resultant copolymer morphologies can be tailored by mixing diblock copolymers and metal containing homopolymers.

Thermal decomposition of organometallic cobalt or iron within a diblock copolymer was reported by Abes et al. The growth of cobalt particles by thermal decomposing organometallic cobalt within P2VP (poly-2-vinyl pyridine) domains of poly(styrene-b-2-vinyl pyridine) was reported.[27]

The magnetic properties of metal nanoparticles depend on the size distribution of the particles, on finite-size effects and on the interparticle interactions which are controlled by the metal concentration and type of polymer template.[1] Most current research is focused on determining the smallest size of magnetic particles that can be successfully used for magnetic recording.[28–30] Surface and core magnetic properties and interface effects such as spin disorder and spin transport control the information storage capability of the particle and affect the performance of thin-film devices e.g. spin valves, spin transistors and spin-dependent tunneling devices.[31] The magnetic properties of fine particles are being intensively studied to understand their size dependent behavior. Below a critical size, magnetic particles become a single domain

in contrast with the usual multidomain structure for bulk magnetic materials[32] and such small particles may exhibit unique phenomena such as superparamagnetism.

In previous work of Sohn et al.,[3] superparamagnetic iron oxide nanoparticles have been characterized in a diblock copolymer. Metal oxide particles produced within polymer matrices were smaller than 10 nm. It is known that there is no control on the particle size when the copolymer-metal salt solution doping mechanism is used unless the system is a diblock copolymer micelle. Polymeric micelles of poly(styrene)-block-poly(2-vinylpyridine) were used as nanocompartments that were loaded with metal cursors by Spatz et al.[33] The metal ions were reduced in such a way that in each micelle particles were of equal size. The method of Spatz et al. is a simple procedure for the preparation of nanodots in a regular pattern. The versatility of their method allows the control on particle size varying between 1 and 15nm. The effect of different block lengths of polystyrene-block-poly(2-vinylpyridine) was observed on the size of Au nanoparticles, dispersed in a polypyrrole matrix by Selvan et al.[34] Gold nanoparticles ranging from 7 to 13nm in size were produced in the polymers by changing the block length.

Arrangement of the magnetic nanoparticles within one of the domains of a block copolymer can lead to collective magnetic behavior of the nanoparticles. Particle size, dispersion within the polymer matrix and particle interactions are important factors for the resultant magnetic properties and on the performance of the magnetic devices.

The focus of this research is the synthesis of novel norbornene based diblock

copolymers and characterization of these microphase separated polymers. The overall aim of the research presented in this thesis is to investigate the mechanism of dispersion of metal oxide nanoparticles within different morphologies of well characterized diblock copolymers. Two different diblock copolymer systems were synthesized by ring-opening metathesis polymerization: (norbornene-deuterated norbornene dicarboxylic acid) and (norbornene methanol-norbornene dicarboxylic acid). The distribution of iron oxide nanoparticles within various diblock copolymer morphologies was studied using several characterization techniques such as transmission electron microscopy and small-angle neutron and x-ray scattering. The effect of polymer compositions on iron oxide particle formation and their effect on polymer morphology and magnetic properties were studied for the series of two different diblock copolymer systems.

1.1 Project Goals

The objectives of this research were:

1. To synthesize self-assembled norbornene based functionalized diblock copolymers with varying volume fractions and morphologies.

2. To examine the pure diblock copolymer morphologies to be used as nanotemplates for the synthesis of magnetic nanoparticles.

3. To investigate the distribution of iron oxide nanoparticles within different morphologies of copolymers and to understand the influence of doping mechanisms on particle dispersion for the effective templating process within the block copolymers.

4. To study the magnetic properties of polymeric inorganic nanocomposites

and understand their structural-magnetic properties. To relate the arrangement of particles and particle size within diblock copolymer templates to the magnetic properties.

5. To understand the influence of particle concentration on the microphase separation of block copolymers. To study the ionic coordination of Fe to the block copolymer in solution and explain the resultant changes in morphologies by ionic interactions in solution and by the formation of ionic aggregates.

The methods used to reach our objectives can be outlined as follows:

1. The deuterated monomer, which was used in both copolymer systems, was synthesized by a Diels-Alder reaction. All the monomers synthesized were characterized by Nuclear Magnetic Resonance Spectroscopy (NMR). Diblock copolymers of (norbornene-deuterated norbornene dicarboxylic acid) and (norbornene methanol-norbornene dicarboxylic acid) with different block ratios were synthesized by ring-opening metathesis polymerization (ROMP). The diblock copolymers were then characterized by Gel Permeation Chromatography (GPC)/Light Scattering (LS) to determine the actual block ratios and molecular weights of the synthesized polymers. Microphase separated structures were examined in Small-Angle Neutron Scattering (SANS) and the variation of domain spacing with block composition was determined. The morphologies of pure diblock copolymers were examined in TEM by staining one of the blocks.

2. Metal oxide nanoparticles were incorporated into these polymer systems using a solution doping technique and their structural and magnetic properties were investigated by Transmission Electron Microscope (TEM), X-ray Photoelectron Spec-

troscopy (XPS), Superconducting Quantum Interference Device (SQUID) magnetometry, Small Angle Neutron Scattering (SANS) and Small Angle X-ray Scattering (SAXS).

3. The effect of different polymer morphologies on metal oxide ordering was examined by SANS, SAXS and TEM. Particle arrangement and particle interactions within diblock copolymer matrices were investigated in conjunction with the examination of their magnetic properties.

4. An alternative doping method consisting of submerging thin films in a metal salt solution was used and its influence on templating iron oxide nanoparticles was explored by comparing to the undoped copolymer morphology. The successful investigation of the undoped copolymer morphologies revealed the effect of different doping mechanisms and the role of self-assembled diblock copolymer matrices in templating nanoparticles.

5. The magnetic properties of metal doped samples were studied through Superconducting Quantum Interference Device (SQUID) magnetometry measurements. The blocking temperatures, saturation magnetization and magnetic behavior of the systems as a function of temperature were determined from magnetization versus field (M-H) and magnetization versus temperature (M-T) experiments. These magnetic characteristics were indicative of the particle size and arrangement within various copolymer structures.

Chapter 2

Block Copolymers and Magnetism

2.1 Diblock Copolymers and Phase Behavior

Equilibrium polymer-polymer phase behavior depends on molecular architecture, choice of monomers, composition and degree of polymerization. Molecular architectures influence polymer mobility and determine the phase morphology. Some possible architectures of polymers are homopolymer mixtures, star block copolymers, graft block copolymers, multiblock copolymers, dendrimers, hyperbranched comb polymers etc. Block copolymers are formed by combining two or more polymers by covalent bonds. The block composition is the overall volume fraction of a component and the degree of polymerization is the number of monomers that makes up the polymer chain. The choice of monomers defines the sign and magnitude of the energy of mixing of the monomers. The interaction parameter, χ, is defined as,

$$\chi = \frac{1}{k_B T}\left[\epsilon_{AB} - \frac{1}{2}(\epsilon_{AA} + \epsilon_{BB})\right] \tag{2.1}$$

where ϵ_{ij} represents the energy of forming i and j segments interactions and k_B is

the Boltzmann constant. A negative value of χ results from a favorable energy of mixing when A-B segment-segment contacts produce a lower energy than A-A and B-B contacts. When the net system energy increases upon forming A-B contacts, the χ value is positive. A phase state is governed by a balance between enthalpic and entropic factors that together constitute the system free energy,

$$\Delta G = \Delta H - T\Delta S \tag{2.2}$$

Flory and Huggins estimated the change in free energy per segment ΔG associated with mixing random walk polymer chains on an incompressible lattice as,[35]

$$\frac{\Delta G}{k_B T} = \frac{\phi_A}{N_A} \ln \phi_A + \frac{1-\phi_A}{N_B} \ln(1-\phi_A) + \phi_A(1-\phi_A)\chi \tag{2.3}$$

The first two terms represent the combinatorial entropy of mixing ΔS. The third term represents the enthalpy of mixing ΔH and it can either decrease or increase the ΔG depending on the sign of χ. The polymer phase diagram depends on the temperature, composition and molecular weight dependence of χ.

2.2 Diblock Copolymers and The Order/Disorder Transition

When χ is positive, a decrease in A-B contacts reduces the system enthalpy H. This process can occur locally segregating A and B blocks. The product χN controls the state of segregation.[36,37]

For $\chi N \ll 10$, entropic factors dominate and diblock copolymers exist in a spatially homogeneous state. When $\chi N = 10$, a balance exists between entropic and energetic effects. Increasing χN induces a first-order transition to an ordered state.[36] This phase transition is called order-disorder transition (ODT). In the limit $\chi N \gg 10$, energetic factors dominate and the ordered microstructures are characterized by narrow interfaces.

The covalent bond between homopolymer blocks prevents phase separation in a macroscopic scale, thus forcing them to microphase separate, depending on the constituent block volume fraction to form spherical, cylindrical and lamellar morphologies (Figure 2.1). As an example, the ordered microstructures for polystyrene-polyisoprene (PS-PI) diblock copolymers are presented on the phase diagram shown in Figure 2.2.

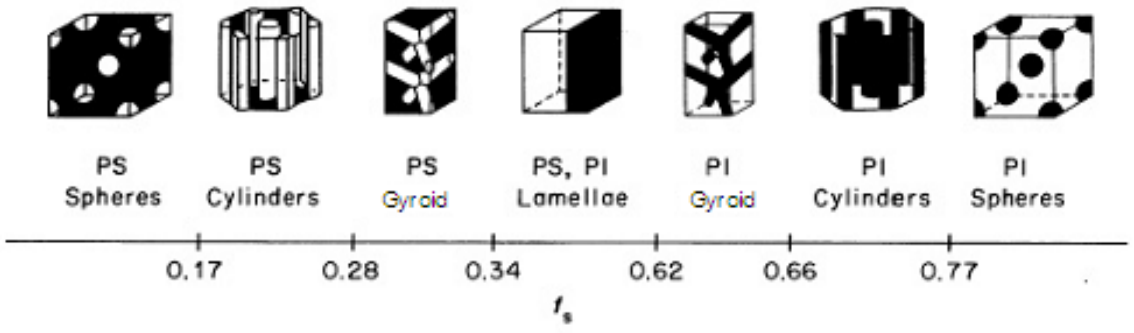

Figure 2.1: Effect of varying volume fractions of the constituent block on the morphologies of polystyrene-polyisoprene diblock copolymer.[36]

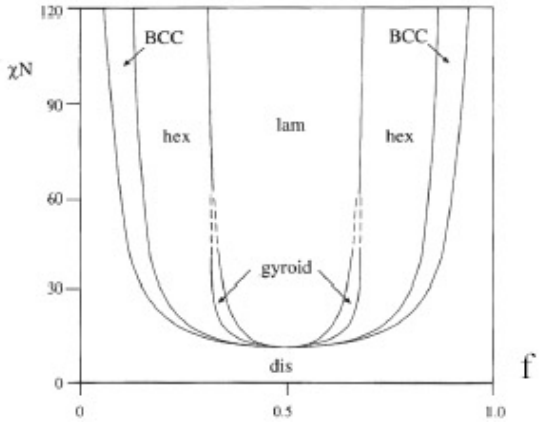

Figure 2.2: Phase diagram for polystyrene-polyisoprene diblock copolymers.

2.3 Ring-Opening Metathesis Polymerization

Ring Opening Metathesis Polymerization (ROMP) is a way of polymerizing strained cyclic olefins using transition metal catalysts. Olefin metathesis consists of the reaction between a transition metal-carbon double bond ($M = CHR$) and an olefin to give a metallocyclobutane ring. ROMP has similarities to chain-growth (free-radical) polymerization where the polymer chain is initiated by a reactive species (such as a free radical), and addition of monomer causes reaction to occur at the reactive end of a growing polymer chain. Living polymerization is a special case of chain growth in which the chain transfer and chain termination steps are very slow compared to the initiation and propagation steps. In living polymerizations, the rate of polymer chain initiation occurs faster than the rate of propagation and all chains grow having the same length. This results in polymers with molecular masses close to the target molecular masses and narrow molecular mass distributions.

ROMP has been used to synthesize functionalized block copolymers with well-

defined architectures and narrow molecular mass distributions. The synthesis of block copolymers with very narrow polydispersity (PDI values lower than 1.1) has been achieved with the introduction of Ru and Mo based catalysts developed by Grubbs and Schrock.[38,39] These initiators can tolerate various functional groups on the monomers such as carboxylic acids, secondary amines, imidazoles, triazoles, triethoxysilyl groups, methyl esters, nitriles in contrast to other polymerization techniques. The metal ligands can be incorporated to these functional groups. Various combinations of monomers of higly-strained cycloolefins like norbornene, norbornadiene, dicyclopentadiene can be polymerized and converted into diblock copolymers by ROMP.[40,41] Molybdenum-based metathesis catalysts can polymerize strained cyclic olefins having polar functional groups; however, their sensitivity to air and water make them difficult for practical use.[42] On the other hand, less strained cycloolefins can be polymerized using a more active catalyst.[43] Addition of a phosphine and a diazo group to ruthenium based catalyst yields highly active catalytic species. The high functional group tolerance of the catalyst system allows the polymerization of several cyclooctene derivatives having acetal, ether, ester, bromine and acid functionalities. A less active catalyst will be more tolerant toward norbornene functionalities.

Stereochemistry determines the rates of initiation and propagation. In our study, functionalized norbornene was added to the polynorbornene catalyzed by Grubbs' catalyst using a method described in Section 3.1.3. The rate of initiation of norbornene-trimethylsilane may be hindered due to steric and electronic effects

with the Grubbs' catalyst during binding of norbornene-trimethylsilane monomer with its bulkier groups. For this reason, the monomers with bulkier groups were added after the simpler monomer was initiated first. The initiation of the less bulky group, norbornene, is faster than the initiation of the norbornene-trimethylsilane monomer. Therefore, we expect to have a narrower polydispersity by initiating the norbornene monomer first. Polymer stereoregularity requires isomeric purity of monomers. The synthesis and characterization of the monomers and polymers are described in Sections 3.1.2 and 3.1.3.

Ring-opening polymerizations are thermodynamically favored for -3, -4, -8 and larger membered ring compounds. When there is a bridging carbon, (ΔG) of the polymerization for the opening of a particular ring will be more negative as the result of an increased strain energy in the monomer.[44] The ROMP of strained cyclic olefins initiated by metal carbene complexes shows the characteristics features of a living polymerization. Therefore block copolymers can be made by sequential addition of different monomers containing bridge carbons such as norbornene.[39]

2.4 Definitions in Magnetism

The spins of a magnetic material align under a sufficiently large magnetic field. The maximum value of the magnetization is achieved when all the spins are aligned and this state is called saturation magnetization (M_s). As the applied magnetic field decreases, spin alignment stops and a decrease in magnetization curve is observed. In ferromagnets, at zero field a residual magnetization is observed which is called remanent magnetization, M_r. The field to bring the magnetization of a ferromagnet

back to zero is called the coercive field, H_c. The shape of the hysteresis curve is important for magnetic recording applications which requires a large remanent magnetization and coercivity[45] (Figure 2.3).

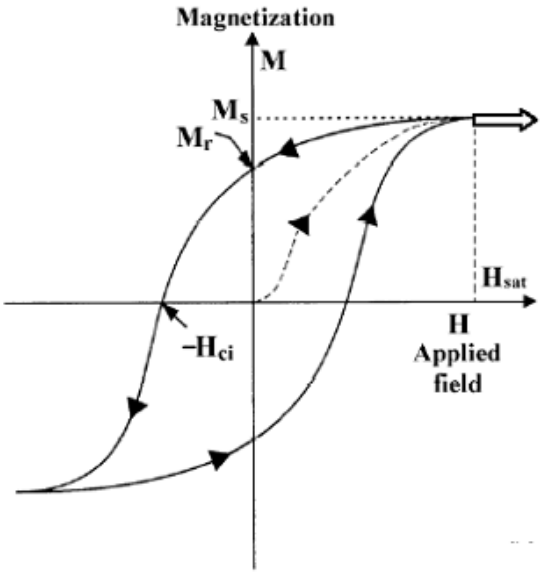

Figure 2.3: The saturation magnetization, M_s, remanent magnetization, M_r and coercivity, H_c are obtained from a magnetic loop.

2.5 Finite-size Effects and Magnetic Properties

Finite-size effects control the magnetic properties of nanoparticles as the particle size decreases. Nanoparticles have a high surface/volume ratio and hence surface effects and particle-polymer interactions play an important role in their magnetic behavior.[46] In bulk magnetic materials, multidomain structures are separated by domain walls which have a characteristic width and energy associated with their formation. The size and shape of the domain walls depend on the exchange, magnetostatic and anisotropic energies. As the volume of the magnetic particles decreases,

the size of the domains, the width of the walls and the magnetostatic energies are reduced. Below a certain critical size, the energy to produce a domain wall is greater than the reduced magnetostatic energy. Consequently, the system does not form smaller domain walls and maintains the magnetic structure of a single domain. As the particle size decreases below the single domain value, the spins move by thermal fluctuations and the system becomes superparamagnetic below a critical size. This critical size depends on the saturation magnetization, anisotropy energy and exchange interactions between the spins. For a single domain particle, the magnetization of a particle points in a direction that minimize its total anisotropy energy. The anisotropy energy keeps the particles magnetized in a particular direction and is proportional to the particle volume.[45] It can be expressed as

$$E(\theta) = KV \sin^2(\theta) \tag{2.4}$$

where θ is the angle between the anisotropy and magnetization axis, K is the effective uniaxial anisotropy energy per unit volume, V is the particle volume and KV is the anisotropy energy barrier. Superparamagnetism is a result of finite-size effects since the particle anisotropy is proportional to its volume. As temperature decreases the thermal energy $k_B T$ becomes comparable to the energy barrier, KV. Above a certain temperature thermal excitations cause spin fluctuations to overcome the single-energy barrier. This temperature is called the blocking temperature, T_b. Below the blocking temperature, the thermal energy is not adequate to flip the moment of the domain within the experimental measuring time and thus spin reversals are blocked and particles exhibit ferrimagnetic behavior. Hysteresis in the M-H (mag-

netization versus field) data should be observed below T_b. The relaxation time (τ) of the magnetic moments due to thermal fluctuations is given by an Arrhenius-like expression as

$$\tau = \tau_0 exp(\frac{KV}{k_B T}) \tag{2.5}$$

where τ_0 is the characteristic measuring time of the instrument, k_B is the Boltzmann constant and T is the temperature. Superparamagnetism is observed above T_b where spin relaxation is rapid compared to the instrument measuring time. The blocking temperature, T_b, depends on the particle size. As particle size decreases, the spins are blocked at a lower temperature resulting in a lower T_b. Equations 2.4 and 2.5 are valid for non-interacting particles.

Superparamagnetism is the limit to information storage. Information is coded through the direction of the particle's magnetization in its blocked state because it is possible to switch the magnetic moment by applying a magnetic field opposite to it. This is the principle of magnetic recording.

2.6 Interparticle interactions

Magnetic interactions between superparamagnetic particles influence the relaxation time of the particles. Magnetic interactions exist as dipole-dipole interactions and exchange interactions between the surface and the core in the nanoparticles. The interactions modify the anisotropic energy barrier contributions of each particle. For non-interacting particles the exchange interaction is ignored, only magnetic dipole in-

teraction exists.[47] The calculation of superparamagnetic relaxation times in systems of interacting particles is a complex problem even for weakly interacting particles. The relaxation times depend on the geometrical arrangement of the particles and on the orientation of the easy directions of magnetization.[48] In the limit of strong interactions, the magnetic energy barriers of individual particles are negligible and only the magnetization of the assembly occurs. The effect of weak interactions is introduced to the Arrhenius expression by the model of Shtrikmann and Wohlfarth[49] in the Vogel-Fulcher law as follows,

$$\tau = \tau_0 exp\ \frac{KV}{k_B(T_b - T_o)} \tag{2.6}$$

where T_o is the effective temperature which accounts for the interaction effects. As the magnetic particle concentration increases or particle distance decreases, the relaxation time increases and results in higher blocking temperatures.[46,47]

In a different theory, Morup defined the magnetic interactions for weak and high regimes.[47] He proposed that at high temperatures and/or for weak interactions, T_b decreases as interactions increase. It was found that dipole fields from the close particles may decrease the energy barrier separating the two energy minima resulting in a faster relaxation. On the other hand, for strong interactions and/or at high temperatures, T_b increases with increasing interactions and a transition from a superparamagnetic to a glassy state occurs.[50,51]

2.7 Surface Effects

Surface effects influence the magnetization of nanoparticles because the particles have a higher ratio of surface to core spins. Surface effects result from the spin disorder due to lower coordination of the surface cations and the existence of the exchange bonds with the impurity atoms. Since the broken bonds destabilize the magnetic order, the nanoparticles can arrange themselves as having a core with regular spin arrangement and a surface layer where the spins are not oriented randomly but are inclined at some angle to their magnetization direction. This is called "non-collinear spin arrangement" or "surface spin disorder".[52] As a result, the magnetization of the surface layer is lower than that of the core spins. The surface and core magnetization influence the magnetic properties of the system. This is another demonstration of a finite-size effect that determines the magnetization of nanoparticles.

The exchange interaction occurs in ferrimagnetic systems through the oxygen ion.[53] Spin disorder has been verified in different nanoparticle assemblies of ferrimagnetic oxides (γ-Fe_2O_3, $NiFe_2O_4$, $CoFe_2O_4$, $CuFe_2O_4$) by Mossbauer spectroscopy and neutron scattering experiments.[46,54–57]

2.8 Magnetic Characterization by Small-Angle Neutron Scattering

Neutrons have a magnetic moment which can interact with the magnetic moment of the atom. Elements of first transition series (Fe, Co, Ni) have incomplete 3-d

shells. Their unpaired electrons give rise to a magnetic moment which interacts with the magnetic moment of the neutron by the dipole moment associated with an electron's spin or by the orbital motion of the electron. The location of magnetic atoms and spatial distribution of magnetic electrons can be found using neutron scattering. In addition, the temperature and field dependence of magnetic moments can be determined. Orbital and spin moments of unpaired electrons contribute to the magnetization density. The Fourier transform of the spin density is defined as the magnetic form factor which contributes to the form factor of structural scattering.

Magnetic scattering can be distinguished from structural scattering. Above the magnetic ordering temperature, there is no contribution of magnetic scattering to the total observed scattering. Below the ordering temperature, the intensity change can be attributed to the contribution of magnetic scattering to the structural scattering.

One method used to subtract the magnetic scattering from the total scattering is alignment of the spins parallel or perpendicular to the scattering vector by applying a magnetic field in these directions. Spins aligned parallel to the neutron beam do not have any magnetic scattering contribution, however when the magnetic moment directions are perpendicular to the beam, magnetic and structural scattering contributions are additive. Magnetic scattering peaks observed in small-angle neutron scattering spectra can contribute to structural peaks or they can be separate peaks. Magnetic scattering contributes to the total scattered intensity I(q) as follows,

$$I(q) \propto \left|\sum b_r e^{iq\cdot r}\right|^2 + \left|\sum p_r e^{iq\cdot r}\right|^2 \tag{2.7}$$

where b_r is the scattering amplitude of the atom at position r. The magnetic scat-

tering amplitude p_r is defined as $p_r = \sigma_r f_r(q) |S_{\perp r}|$ where $f_r(q)$ is the magnetic form factor and $S_{\perp r}$ is the geometrical factor that represents the component of the moment perpendicular to the scattering vector direction.[58]

Neutron scattering measures the Fourier transform of the pair-correlation function in space and time. Magnetic correlation lengths describe the spin pair correlations which depend on dipolar and exchange forces within the particle and can be analyzed as a function of temperature to observe the effect of spin alignment at the surface.[59] Using Lorentzian fits, correlation lengths can be found using the relation

$$I(q)^{-1} = \frac{q^2\xi^2 + 1}{I(0)} \tag{2.8}$$

where ξ is the magnetic correlation length and I(0) is the intensity at $q = 0$.

Chapter 3

Structural and Magnetic Characterization of Norbornene-Deuterated Norbornene Dicarboxylic acid Diblock Copolymers Doped with Iron Oxide Nanoparticles

Block copolymers which microphase separate into ordered morphologies such as lamellar, cylindrical and spherical microdomains provide a self-assembled template for the synthesis of nanocomposites. These microdomains serve as nanoreactors within which a variety of nanoparticle clusters can be synthesized. In earlier studies, non-magnetic nanoparticles (Au, Ag, Pd, Pt, Cu)[9,16,60–62] and semiconductor nanoclusters (PbS, CdS, ZnS)[10,21,22] were synthesized in norbornene diblock copolymers. The synthesis and characterization of magnetic Fe_2O_3 nanoparticles within a single block copolymer composition, $NORCOOH_{30}MTD_{300}$, (NORCOOH: 2-norbornene-5, 6 dicarboxylic acid; MTD: methyltetracyclododecene) were reported by Sohn et al.[3,19] Synthesis of $CoFe_2O_4$ nanoparticles within $NOR_{400}NORCOOH_{150}$ (NOR: norbornene) polymer was also reported for one diblock copolymer morphology.[63] Both

studies discuss the synthesis and the morphology of the magnetic oxide nanoparticles formed from templating a single block copolymer composition. We report the effect of constituent block composition variations on the templating, morphology, and magnetic properties of resultant magnetic nanoparticles formed within diblock copolymer matrices. The major investigative tool, small-angle neutron scattering requires that one of the constituent blocks of the block copolymer be deuterated. The objective of this study is to analyze the effect of various copolymer morphologies on nanoparticle dispersion and magnetic properties by characterizations of metal oxide doped polymers through Transmission Electron Microscopy (TEM), Small-Angle Neutron Scattering (SANS) and Superconducting Quantum Interference Device (SQUID) magnetometry.

3.1 Experimental

3.1.1 Materials

Norbornene (99%) was purchased from Fischer Scientific and distilled over sodium under argon and degassed before use. Ethyl vinyl ether, dichloromethane (CH_2Cl_2), deuterated fumaric-2,3-D_2 acid (98 atom % D) and anhydrous ethanol were purchased from Aldrich. CH_2Cl_2 was distilled over calcium hydride under argon. Bis(tricyclohexyl phosphine) benzylidine ruthenium(IV) dichloride (Grubbs' catalyst) was purchased from Strem Chemicals. All solvents, monomers and catalysts required for polymer synthesis were stored inside an MBraun LabMaster100 glovebox. A stock solution of Grubbs' catalyst was prepared by dissolving 1 g of the catalyst in 20 mL

dichloromethane (CH_2Cl_2) and stored at -20 °C inside the glovebox.

3.1.2 Monomer Synthesis

Deuterated 2-norbornene-5,6 dicarboxylic acid (NORCOOH) was synthesized through a Diels-Alder reaction. Cyclopentadiene was obtained from dicyclopentadiene cracking at 180 °C. Deuterated fumaric acid (5g, 0.043 mole) was first dissolved in 250 ml ethanol. When the solution became clear, freshly cracked cyclopentadiene (2 molar eq.) was added to this solution. The reaction was complete in 12 hours. The reaction scheme is shown in Figure 3.1. Ethanol was stripped off, then the white precipitated solid was dissolved in pentane and ether respectively to remove the unreacted components. The white solid was dried at 50 °C oven for 3 days. The yield of deuterated norbornene-dicarboxylic acid was 84%. A ^1H NMR of the compound is shown in Figure 3.2. The chemical shifts of the NMR spectrum are presented in Table 3.1.

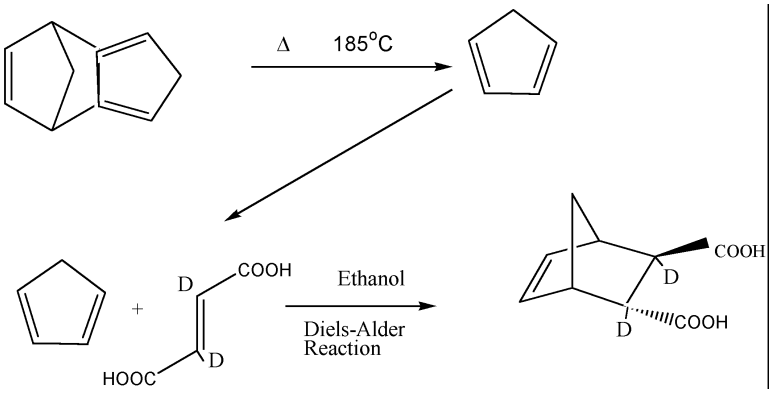

Figure 3.1: Synthesis of deuterated-norbornene dicarboylic acid.

Deuterated 2-norbornene-5,6 dicarboxylic acid (13.45g, 0.073 mole) was dissolved in 500 ml anhydrous ether. The reaction flask was purged with argon and anhydrous

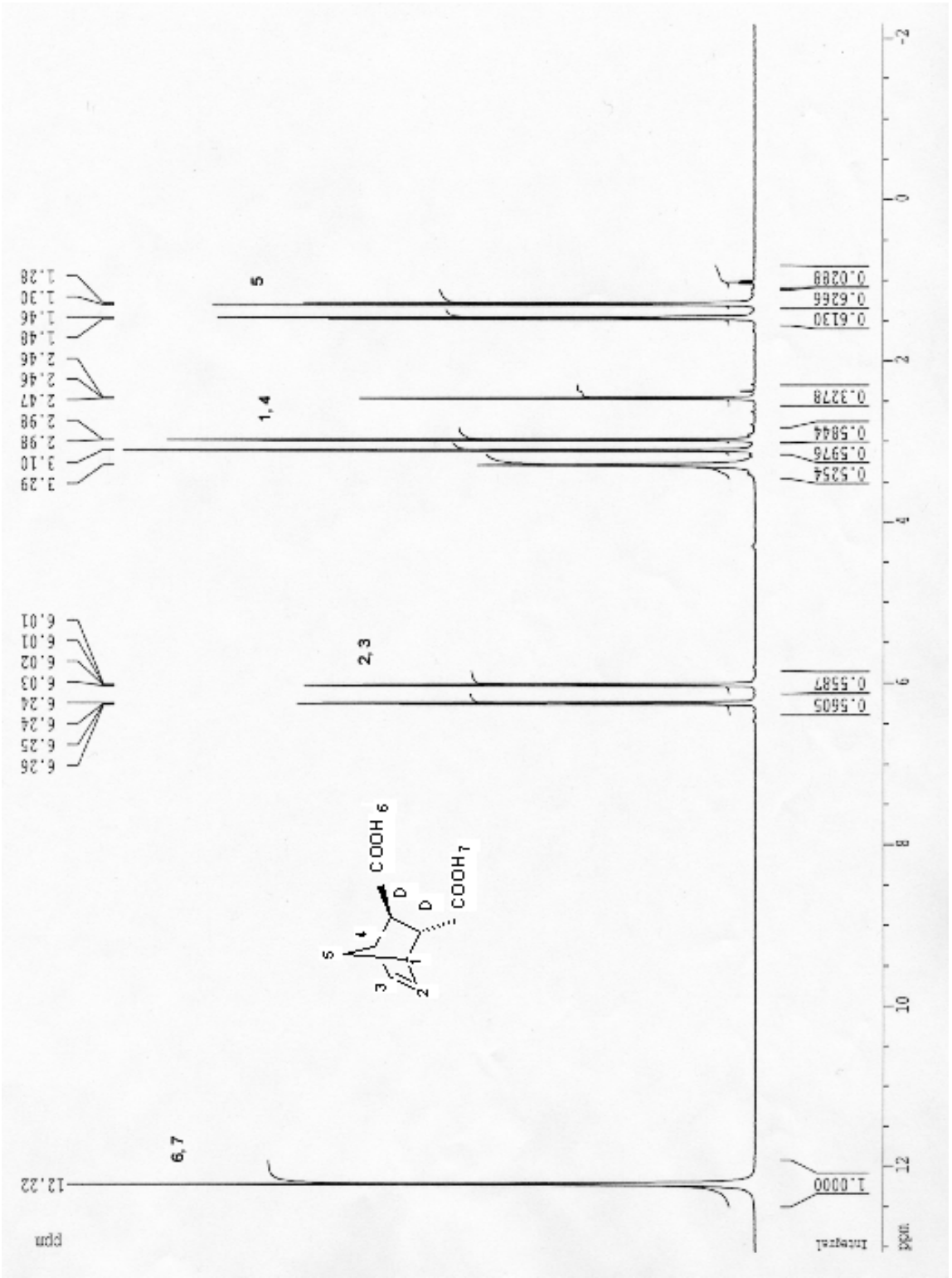

Figure 3.2: ^1H NMR of deuterated NORCOOH in d-THF.

Positions	Type of bonds	Shifts (ppm)
1,4	CH, multiplet	2.98-3.29
2,3	Olefinic, =CH, multiplet	6.01-6.26
5	Bridge head, CH, broad singlet	1.28-1.30
6,7	COOH	12.22

Table 3.1: ^1H-Chemical shifts of the NMR of deuterated NORCOOH.

pyridine (11.45g, 0.146 mole) was added to the reactor in one shot. Chlorotrimethylsilane (15.86 g, 0.146 mole) was added to the flask and was stirred for 3 hours under an argon atmosphere. A white precipitate of pyridine hydrochloride salts was formed immediately after the chloro-trimethylsilane injection.[64] The reaction scheme is shown in Figure 3.3. After 3 hours, the solution was passed through celite to remove pyridine hydrochloride salts. This solution was stripped off ether and the white crystals obtained were dissolved in pentane and passed through celite for a second time. These filtrations were done in a glove bag under argon. After stripping the solvent, purification of the norbornene-dicarboxylic acid-bis trimethylsilylester was carried out via 4 crystallization steps. Two crystallizations in pentane and two crystallizations in ether were done at -20 °C in the glove box to obtain white crystals.

A ^1H NMR of the compound is shown in Figure 3.4. The chemical shifts are presented in Table 3.2.

3.1.3 Polymerization

Ring-opening metathesis polymerization (ROMP) has been used to synthesize functionalized block copolymers with well-defined architectures and narrow molecular

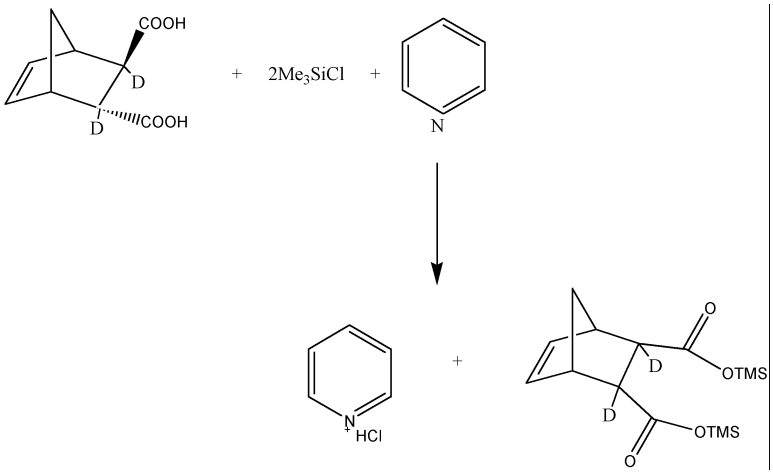

Figure 3.3: Synthesis of deuterated-norbornene dicarboylic acid trimethylsilylester

Positions	Type of bonds	Shifts (ppm)
1,4	CH, multiplet	2.82-2.93
2,3	Olefinic, =CH, multiplet	5.80-6.02
5	Bridge head, CH, broad singlet	1.13-1.34
6,7	TMS	0

Table 3.2: ^1H-Chemical shifts of the NMR of deuterated NORCOOTMS.

weight distributions. In our study, deuterated diblock copolymers were synthesized by sequential polymerization of norbornene (NOR) followed by deuterated norbornene dicarboxylic acid (NORCOOH). The first generation Grubbs' catalyst was used in the polymerization of the norbornene homopolymer. Polymer synthesis was conducted according to literature procedures.[18] All polymerizations were performed in the glove box under nitrogen at room temperature. In a typical polymerization, a 0.2 mmol/mL solution of norbornene was prepared in CH_2Cl_2 and an equivalent amount of catalyst was added. Norbornene-TMS solution was added to the norbornene homopolymer solution after 1 hour. The amount of monomers and

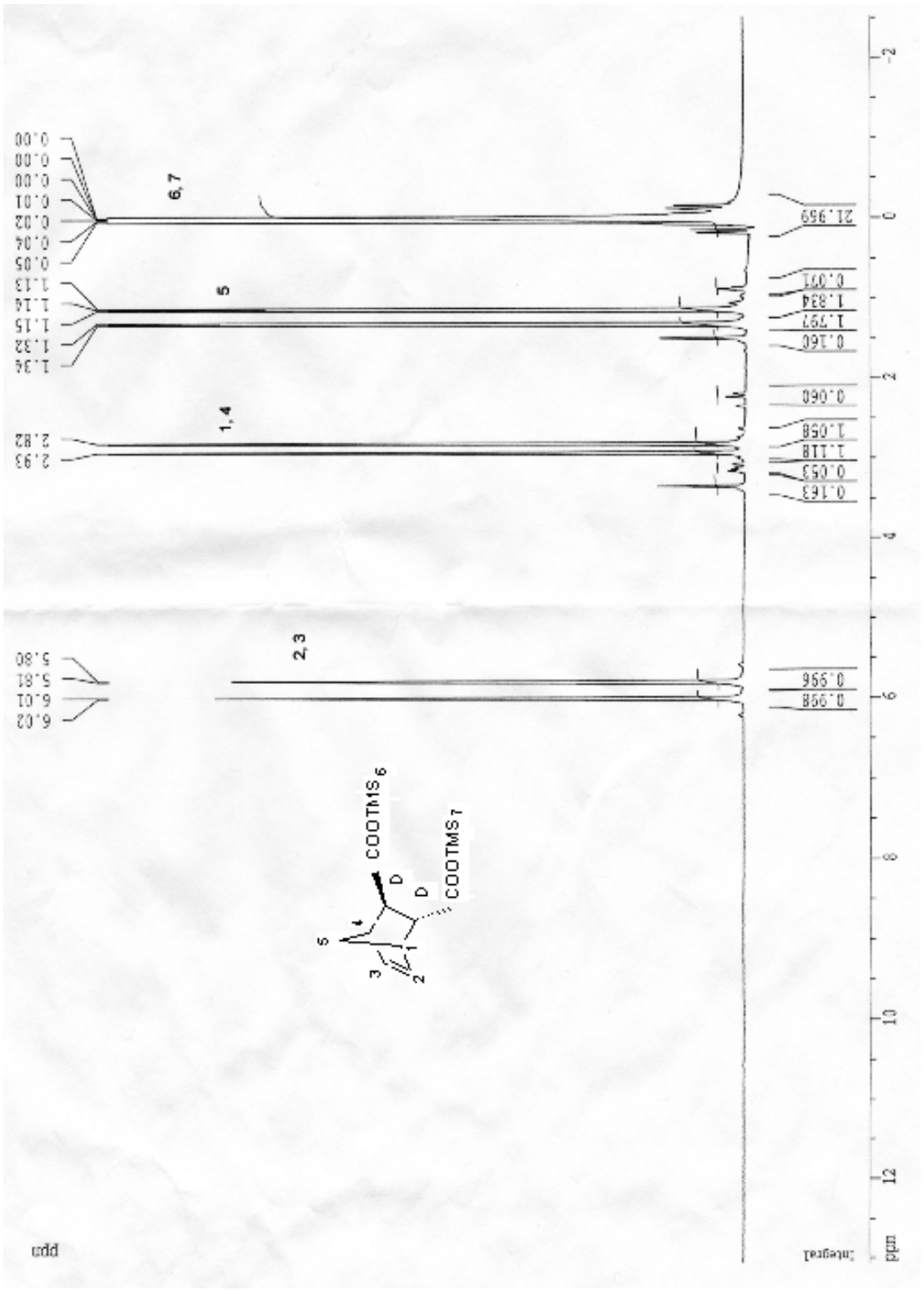

Figure 3.4: ^1H NMR of deuterated NORCOOTMS in $CDCl_3$.

catalyst used in the synthesis of the series of diblock copolymers are shown in Table 3.3. Target compositions presented in Table 3.3 are the stoichiometric monomer amounts added to the reaction mixture, they do not represent the actual composition of the diblock copolymers. The diblock copolymer consists of NOR_x/deuterated-$NORCOOH_y$ where x and y are the repeating units. The polymerization scheme is shown in Figure 3.5. x and y values were determined by measurement of the refractive index change by concentration (dn/dc) and gel permeation chromatography-light scattering analysis. The yields of the deuterated diblock copolymers were determined to be 96% for NOR_{360}/$NORCOOH_{120}$; 83% for NOR_{320}/$NORCOOH_{190}$ and 91% for NOR_{290}/$NORCOOH_{260}$.

Target Composition	NOR(mole)	NOR-TMS(mole)	Catalyst(mole)
400/100	0.0106	0.00265	$2.65 * 10^{-5}$
400/150	0.0106	0.0039	$2.65 * 10^{-5}$
400/200	0.0106	0.0053	$2.65 * 10^{-5}$

Table 3.3: Stoichiometric monomer and catalyst amounts for polymerizations of norbornene-(deuterated) norbornene dicarboxylic acid block polymer.

The polymerization times for various diblock norbornene polymers were determined by Gel Permeation Chromatography (GPC) measurements of polymer aliquots at different times. The polymerization times for the series of copolymers of target composition (400/100, 400/150 and 400/200) were 22 hours, 24 hours and 48 hours, respectively. Polymerizations were terminated by addition of ethyl vinyl ether. The polymer solution was stirred for an hour to make sure that termination was completed and then precipitated in a pentane, acetic acid and deionized water

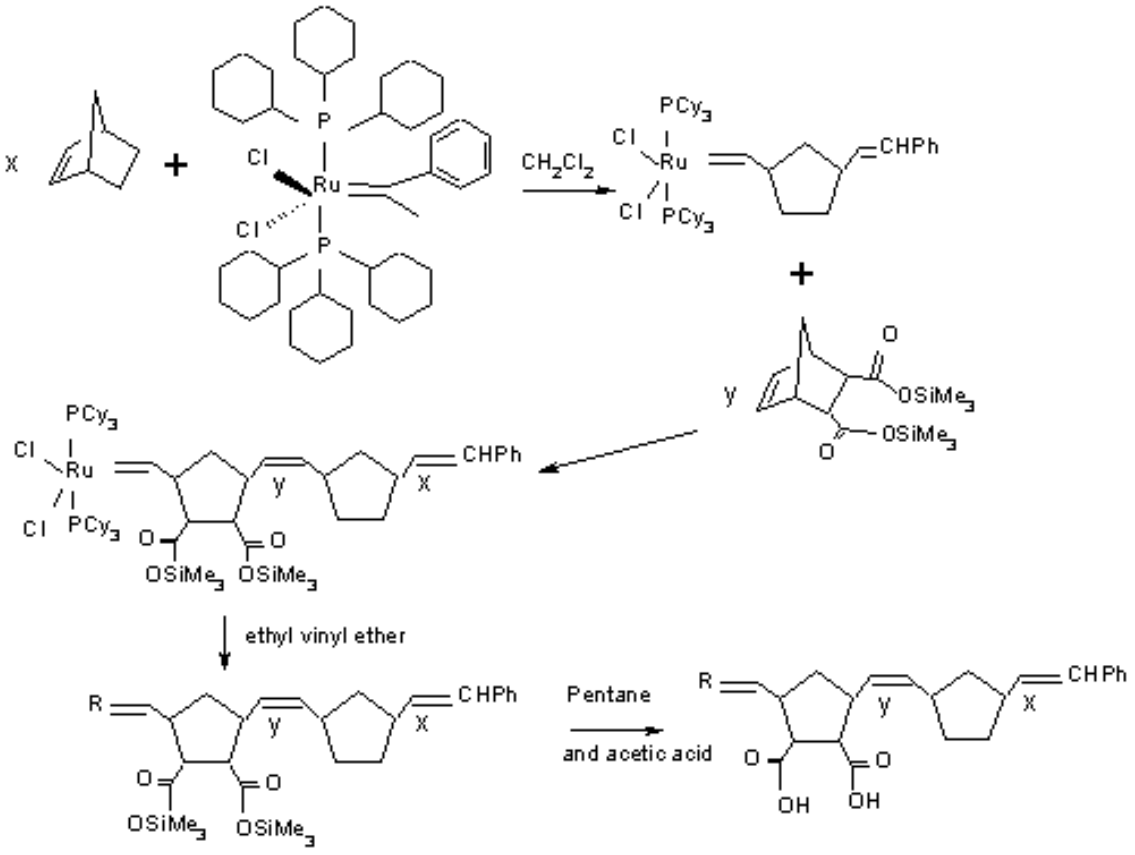

Figure 3.5: Ring-opening metathesis polymerization of $[NOR]_x[NORCOOH]_y$.

mixture to hydrolyze the trimethyl silane groups. The precipitated polymer was dried under vacuum for 24 hours.

3.1.4 Incorporation of Iron Oxide Nanoparticles into Diblock Copolymers

The carboxylic acid groups of norbornene-deuterated norbornene dicarboxylic acid diblock copolymer solution in tetrahydrouran (THF) (3 wt%) were associated with the required amount of iron salts in THF (ion exchange reaction between $FeCl_3$ and NORCOOH requires a 1:1 Fe^{+3}:COO^{-1} molar ratio) at room temperature overnight. Polymers containing the iron salts were static solution cast on teflon covered aluminum cups. The solvent was slowly evaporated and the films were dried for 6 days. The films were soaked in 2 M NaOH solutions to produce Fe_2O_3 particles and then washed with water. Elemental analysis of Fe-doped polymers after the washing step indicated that the iron amount in the samples had decreased after the washing step (Table 3.4), which indicated that some Fe ions were not associated with the carboxylic acid groups during iron doping.

Sample	wt% Fe before washing	wt% Fe after washing
360/120	7.4	6
320/190	9.4	7
290/260	11.7	10

Table 3.4: Fe amounts in wt% before and after washing iron oxide doped diblock copolymer films.

3.2 Characterization Techniques

Molecular weight distributions and absolute molecular weights were measured by Gel Permeation Chromatography/Light Scattering (GPC/LS) using a Wyatt Technology Mini-DAWN light scattering detector, a Waters 2410 RI detector and a Waters 515 pump and a Rheodyne 7125i injector with a 200μL loop. The mobile phase was tetrahydofuran (THF) with 1 ml/min flow rate. Waters styragel 10^4Å 10^5Å and 10^6Å columns were used for these measurements.

The morphologies of the metal oxide doped polymers and metal oxide particle sizes were examined by TEM (Hitachi H-600, operated at 100keV). TEM samples were prepared by ultramicrotoming using a diamond knife.

Magnetic characterization was performed by superconducting quantum interference (SQUID) measurements. The temperature dependence of the magnetization was determined by zero field-cooled (ZFC) and field-cooled (FC) measurements. The ZFC curve was obtained by cooling down to 5K at zero field and then measuring the magnetization under a 200 Oe applied magnetic field. The magnetization was measured during heating from 5K to room temperature at 5K intervals. The FC curve was similarly obtained except that this time the sample was cooled while applying a 200 Oe magnetic field.

Small angle neutron scattering experiments were carried out at the Center for Neutron Research at the National Institute of Standards and Technology (NCNR) on the 8-meter NG1[65] instrument. 10Å wavelength neutrons were used. The sample to detector distance was set to 3.84 cm and the detector angle was 3.5°.

X-ray photoelectron spectroscopic measurements were performed using a Kratos

Axis 165 spectrometer at a vacuum of 4x10^{-10} Torr with nonmonochromatic Mg Kα radiation. All measurements were done in electrostatic mode, with a step size of 0.1 eV and sweep time of 60 s. All individual region spectra are recorded in the Fixed Analyzer Transmission analyzer mode with pass energy of 20 eV.

3.3 Results and Discussion

The microstructure of iron oxide particles was determined by X-ray Photoelectron Spectroscopy (XPS). After subtraction of a linear background, all spectra were fitted using 60% Gaussian/40% Lorentzian peaks, taking the minimum number of peaks consistent with the best fit. The important parameters in the fitting process are peak position, full width at half maximum, intensity and the Gaussian fraction. The high resolution Fe 2p spectrum of the sample is shown in Figure 3.6. The main Fe(2p 3/2) structure is a broad peak with a full width at half maximum of about 3.8 eV. Since the asymmetric structure is clear in this peak envelope, it has been resolved to various components as described by Zetaruk et al.[66] The peak envelope is fit by a series of peaks of decreasing intensity constrained to similar width and shape. Analysis of the two main peaks in the Fe (2p 3/2) envelope has shown that spin orbit splitting is 1.0 eV, which matches exactly the value reported for γ-Fe_2O_3 in the literature.[66] Earlier calculations and studies have shown that both α-Fe_2 O_3 and γ-Fe_2O_3 yield similar intensity distributions for the Fe(2p 3/2) peak envelope. The spin orbit splitting is 1.2eV for α-Fe_2O_3 where as γ-Fe_2O_3 has a splitting of 0.2eV less than α-Fe_2O_3. We therefore conclude from the XPS data that the iron oxide is present as γ-Fe_2O_3. A small contribution of Fe_3O_4 was seen in the Fe(2p

3/2) envelope at 708 eV.

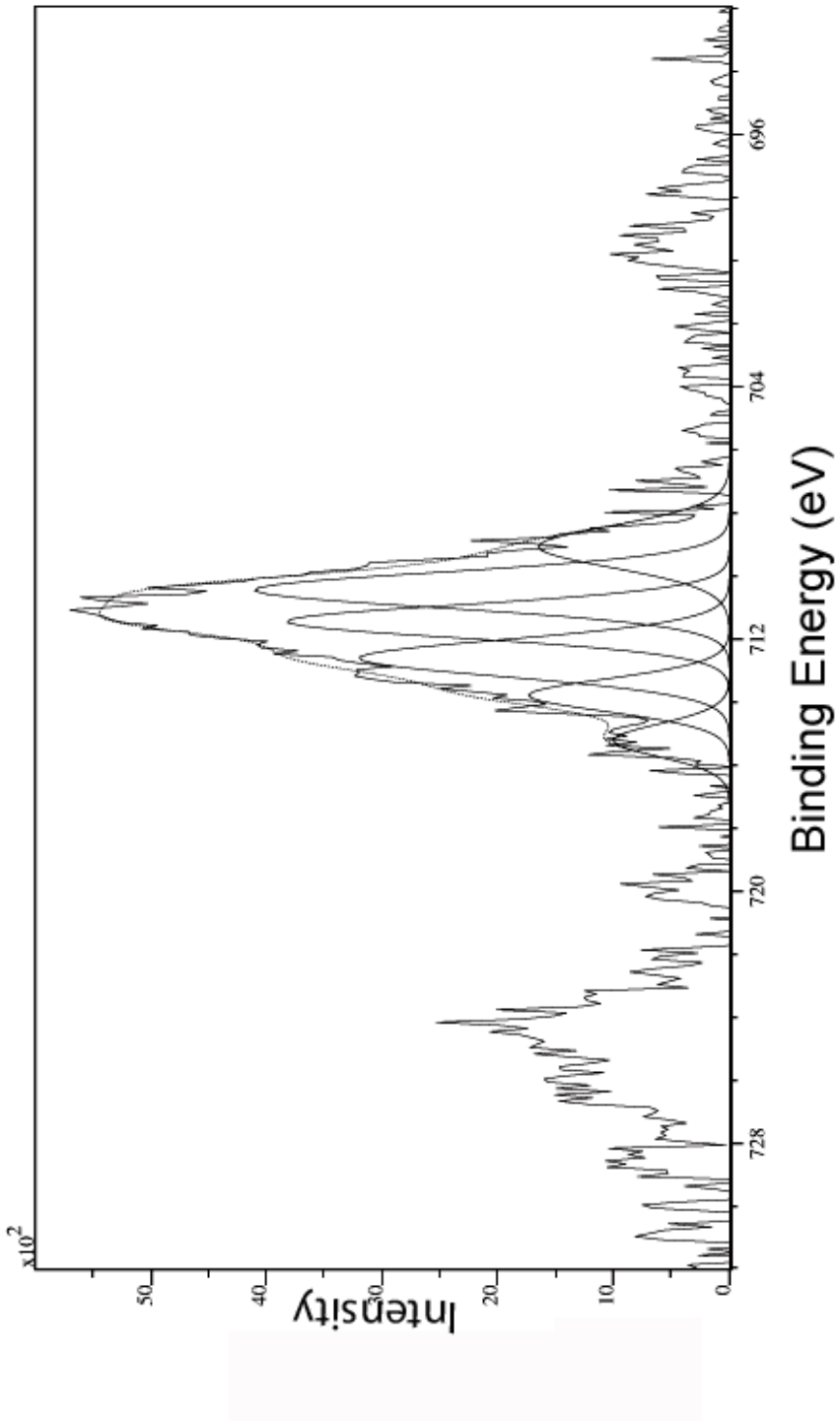

Figure 3.6: XPS spectra of γ-Fe_2O_3 nanoparticles in $NOR_{360}NORCOOH_{120}$.

3.3.1 Molecular Weight Determination

The molecular weights of the first and second blocks are analyzed using GPC/LS. The measurement of the molecular weights of both blocks, allows the number of monomer repeating units in each constituent blocks to be computed.

The differential refractive index, dn/dc, of a polymer/solvent pair is an important parameter for the absolute molecular weight determination where a refractometer is used to determine sample concentrations. dn/dc values for each composition of copolymers in THF were measured using a differential refractometer. Polymer samples of varying concentrations (1-10mg/ml) were run through the refractometer and the raw data (voltage) was read from the detector. The change in the refractive index is expressed as $\Delta n = \Delta V d(\Delta n)/d(\Delta V)$ where $d(\Delta n)/d(\Delta V)$ is the calibration constant. The calibration constant was measured from a polystyrene standard with a known dn/dc. dn/dc values were calculated from the slope of Δn versus concentration change (Δc). In an earlier study, it was reported that refractive index increases as the humidity increases and it is very sensitive to the hygroscopic content of the samples.[67] In our experiments, depending on the amount of water in THF and polymers, the dn/dc values varied as shown in Table 3.5. The elemental analysis of the polymers gave us the approximate block ratios which were calculated from the weight percentages of each element. This time dn/dc values were predicted from the block ratios found from the elemental analysis using the software to analyze the GPC data. Poly-dispersity index (PDI) values of diblock copolymers and dn/dc values from the elemental analysis results are presented in Table 3.6. Actual molecular weights, block ratios, polymer compositions and molecular weight distributions were

determined from the analysis of GPC/LS data as shown in Table 3.7.

Stoichiometric Block copolymer composition	dn/dc
400/100	0.066
400/150	0.042
400/200	0.040

Table 3.5: dn/dc values of a series of norbornene diblock copolymers measured using a refractometer.

Stoichiometric Block copolymer composition	dn/dc	PDI
400/100	0.040	1.67
400/150	0.044	1.24
400/200	0.021	1.36

Table 3.6: dn/dc values of a series of norbornene diblock copolymers (calculated from the elemental analysis results.)

Total Polymer MW (g/mole)	NOR/NORCOOH Polymer composition	PDI $(\overline{M}_w/\overline{M}_n)$	$\phi_{NOR/NORCOOH}$
55941	360/120	1.67	0.64/0.36
65074	320/190	1.24	0.50/0.50
75146	290/260	1.36	0.40/0.60

Table 3.7: Measured molecular weights, compositions, PDI and volume fractions (ϕ) of a series of norbornene diblock copolymers.

3.3.2 Characterization of Diblock Copolymers Using SANS

Structure analysis is based on the diffraction of X-rays, electrons and neutrons. Diffraction is produced by the interference of waves scattered by an object. When neutrons scatter from the nuclei, changes in wave vector and energy of the neutrons provide structural information about the sample. Neutron scattering can be explained with a classical Bragg diffraction experiment where neutrons scatter by the lattice planes in a crystalline sample as shown in Figure 3.7. The neutron beam is sent to the sample, and the scattered wave from each nucleus spreads out in all directions and the detector collects the scattered beam of neutrons. Neutrons travel an extra distance of $2d\sin(\theta/2)$ between two planes. θ is the scattering angle and d is the distance between the planes. If the scattered waves are in phase, constructive interference of the radiation from the planes occurs when the path difference is an integer of the incident beam wavelengths (nλ).[68]

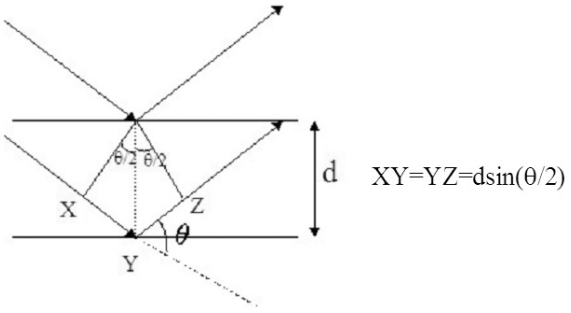

Figure 3.7: Diffraction from crystalline planes.

$$n\lambda = 2d\sin(\theta/2) \tag{3.1}$$

The incidence and final wavevectors have magnitude of $2\pi/\lambda$ and are expressed as k_i and k_f, respectively. The direction change between the incidence and final vectors is

called the scattering vector and written as $q = k_f - k_i$. A schematic of wavevectors and momentum transfer (q) is presented in Figure 3.8.

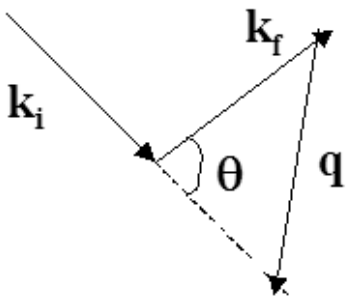

Figure 3.8: Relationship between wavevectors and momentum transfer for elastic scattering.

The scattering vector can be expressed as

$$q = 2k_i \sin(\theta/2) = (4\pi/\lambda)\sin(\theta/2) \tag{3.2}$$

Substituting the wavelength expression in terms of θ (Eqn.3.1) into the scattering vector expression (Eqn.3.2), the relationship between the scattering vector and the crystal lattice spacing

$$q = n2\pi/d \tag{3.3}$$

is obtained.

Variations in neutron scattering length provide contrast for neutron scattering and isotopic labelling can be used to provide this contrast. Since the scattering lengths of hydrogen ($-3.74x10^{-13}cm^{-1}$) and deuterium ($6.67x10^{-13}cm^{-1}$) are very different, diblock copolymers with one block labelled with deuterium can be synthesized to

provide the contrast for a neutron experiment. By labelling one of the blocks of the copolymer, one can learn information about structural arrangements within the diblock. The neutron scattering contrast between the two monomers of the synthesized block copolymer and iron oxide are presented in Table 3.8.

	Neutron Contrast (k_N)
NOR/d-NORCOOH	8.52E-5
NOR/Fe_2O_3	7.14E-3
d-NORCOOH/Fe_2O_3	5.67E-3

Table 3.8: Neutron scattering length density contrasts between monomer-monomer and monomer-iron oxide.

In this study, the NORCOOH block was deuterated to provide contrast between the two blocks for SANS. The neutron scattering data for each sample plotted as Intensity (I) versus scattering vector (Q) is shown in Figure 3.9. Peak positions observed in the SANS data shifted to higher Q values with increasing NOR content, which indicated increasing separation of block copolymer domains and potential changes in morphology. The domain spacing, which is the average center-to-center distance of the microphase separated diblock copolymer domains, was calculated from the peak positions maxima ($d=2*\pi/Q$).

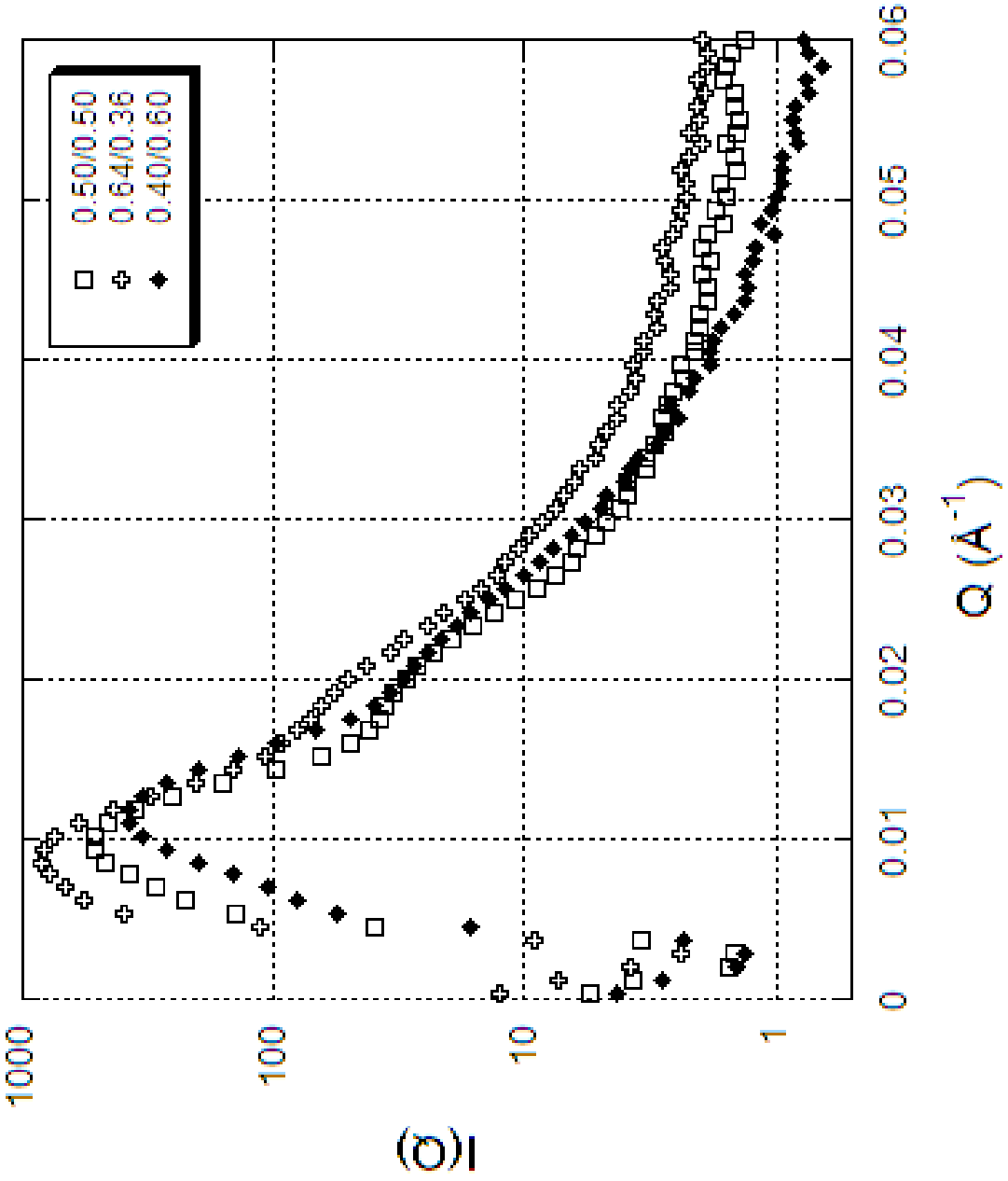

Figure 3.9: SANS profiles of the series of norbornene/deuterated norbornene dicarboxylic acid block copolymers.

SANS experiments with metal oxide doped polymers were performed using the same experimental configurations as for the undoped polymer samples. A change in the shape of the scattering profiles of metal oxide doped polymers (Figure 3.10) was

observed when compared to that of the undoped polymers. These profiles represent the combined scattering from both the polymer domains and magnetic particles at room temperature. Spin dependent magnetic scattering cannot be observed above the ordering temperature, which is around 10K for these systems. Magnetic and nuclear scattering contributions can in general be separated by conducting scattering experiments below the ordering temperature[69] or by performing experiments with polarized neutrons.[70] In our study, only the nuclear scattering from Fe_2O_3 nanoparticles contributed to the scattering from the polymer domains. The correlation of the nuclear scattering from magnetic and polymer parts gives the overall scattering profile.

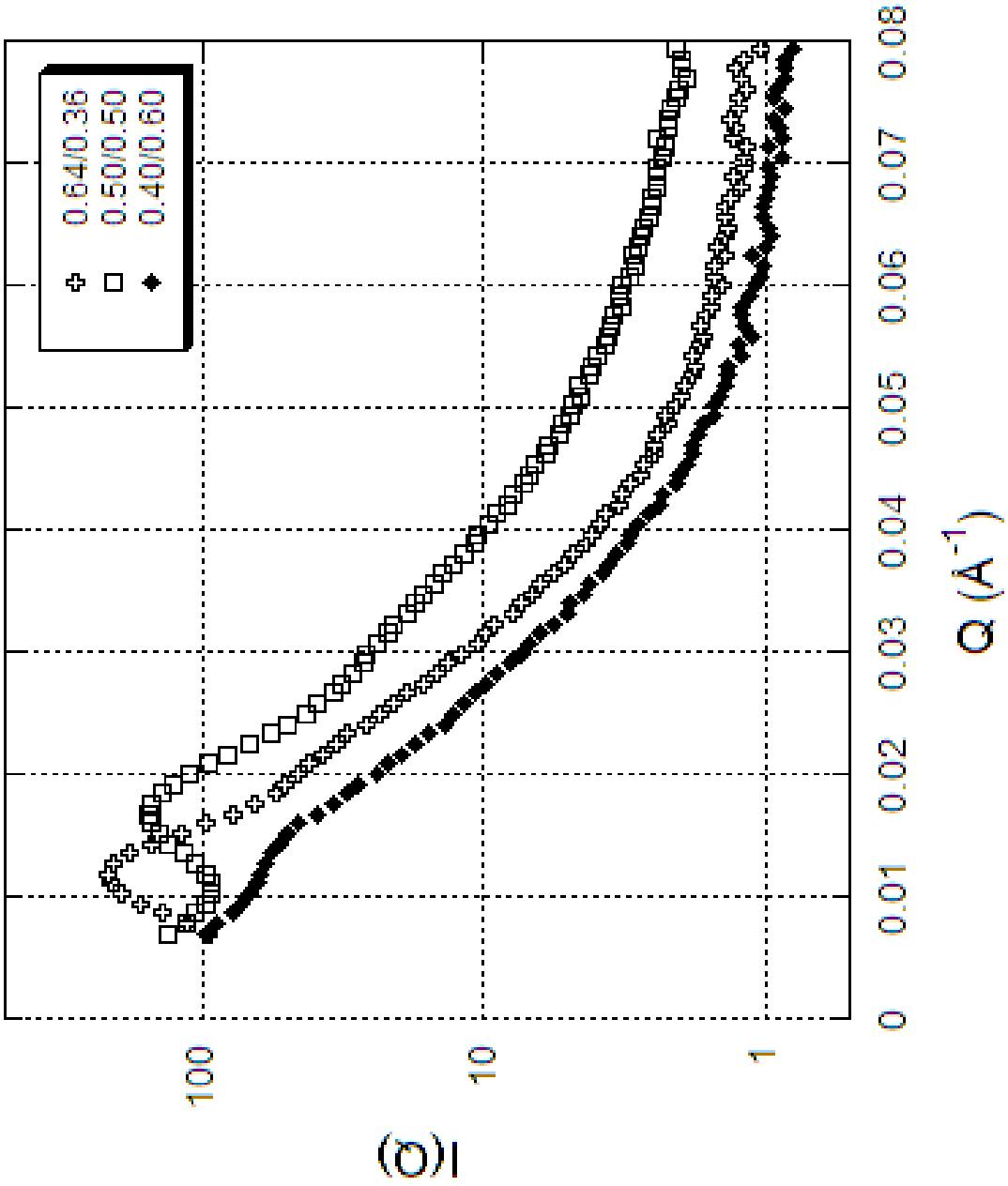

Figure 3.10: SANS profiles of the series of norbornene/deuterated norbornene dicarboxylic acid block copolymers with iron oxide nanoparticles.

The domain spacing obtained by the Q_{max} values of the SANS curves of the metal oxide doped polymers refers to scattering contributions of the underlying microphase separated polymer domains, combined with any scattering from the metal

oxide nanoparticles. The domain spacings calculated from the peak positions of undoped and metal oxide doped samples are shown in Table 3.9 for comparison. Figure 3.11, Figure 3.12 and Figure 3.13 display the scattering profiles of undoped and doped samples at increasing Fe concentrations. The samples with 6 and 7wt% Fe present peaks at doped and undoped states. In these samples, particles were relatively ordered within polymer structure keeping the microphase separated structures. On the other hand, in the sample containing 10 wt% Fe, particles were not well ordered in the polymer matrix and polymer did not retain its original structure. The absence of a peak in the observed scattering from the metal oxide doped sample indicated the disordered structures of iron oxide particles at this concentration. The arrangement of the particles was not controlled with the polymer template at high Fe concentrations. The disordered morphology of the particles was also confirmed in the electron micrographs. The higher the concentration of the Fe particles, the more interconnected structures have been observed.

$\phi_{NOR/NORCOOH}$	$d_{undoped} = 2 * \pi/Q$, $\mathring{A}$	d_{doped} , $\mathring{A}$
0.64/0.36	730	530
0.50/0.50	670	375
0.40/0.60	530	439

Table 3.9: D-spacings for series of undoped and doped diblock copolymers with Fe_2O_3.

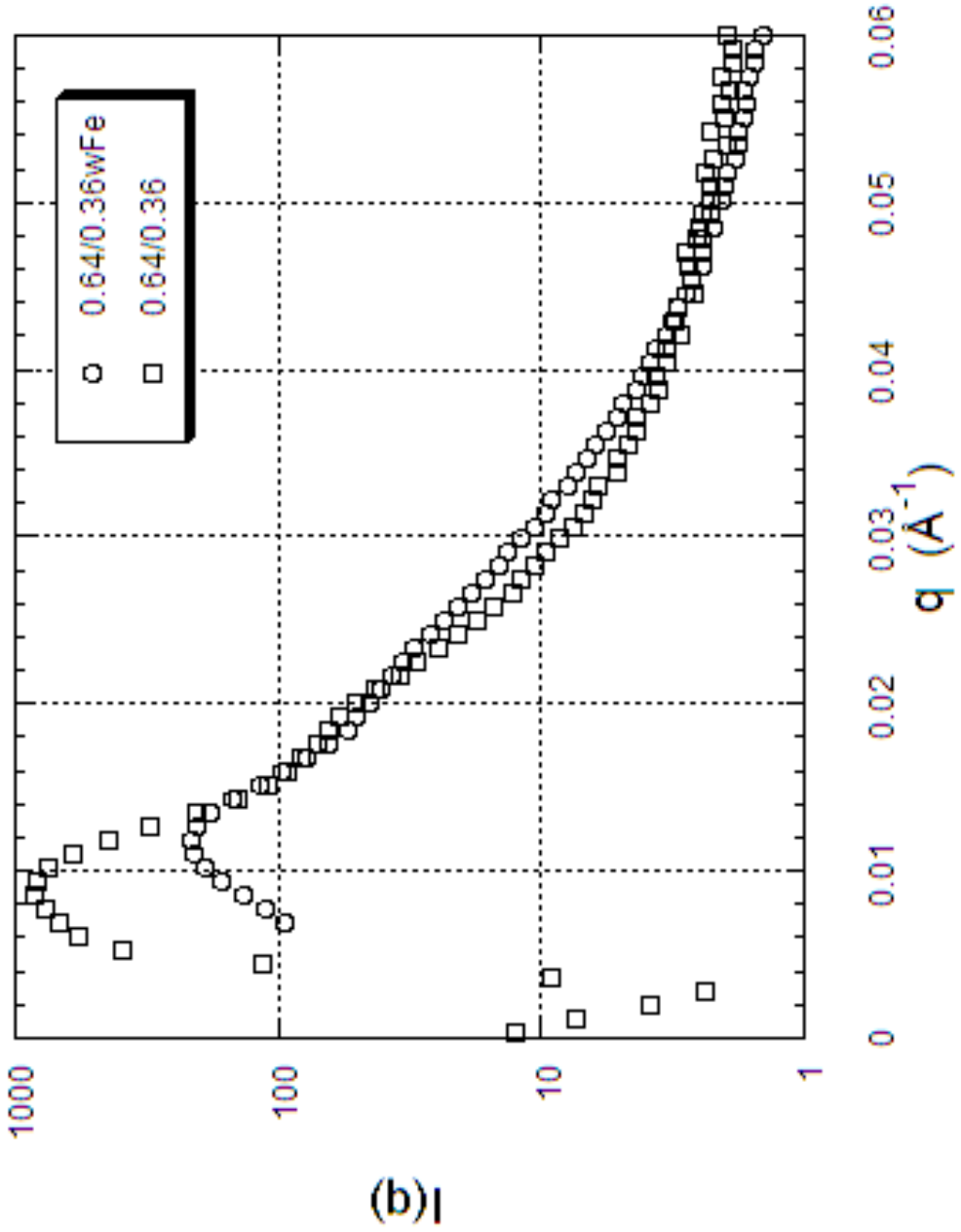

Figure 3.11: SANS profiles of the undoped and doped norbornene/deuterated norbornene dicarboxylic acid block copolymer with volume fraction of 0.64/0/36. The doped sample contains 6 wt% Fe.

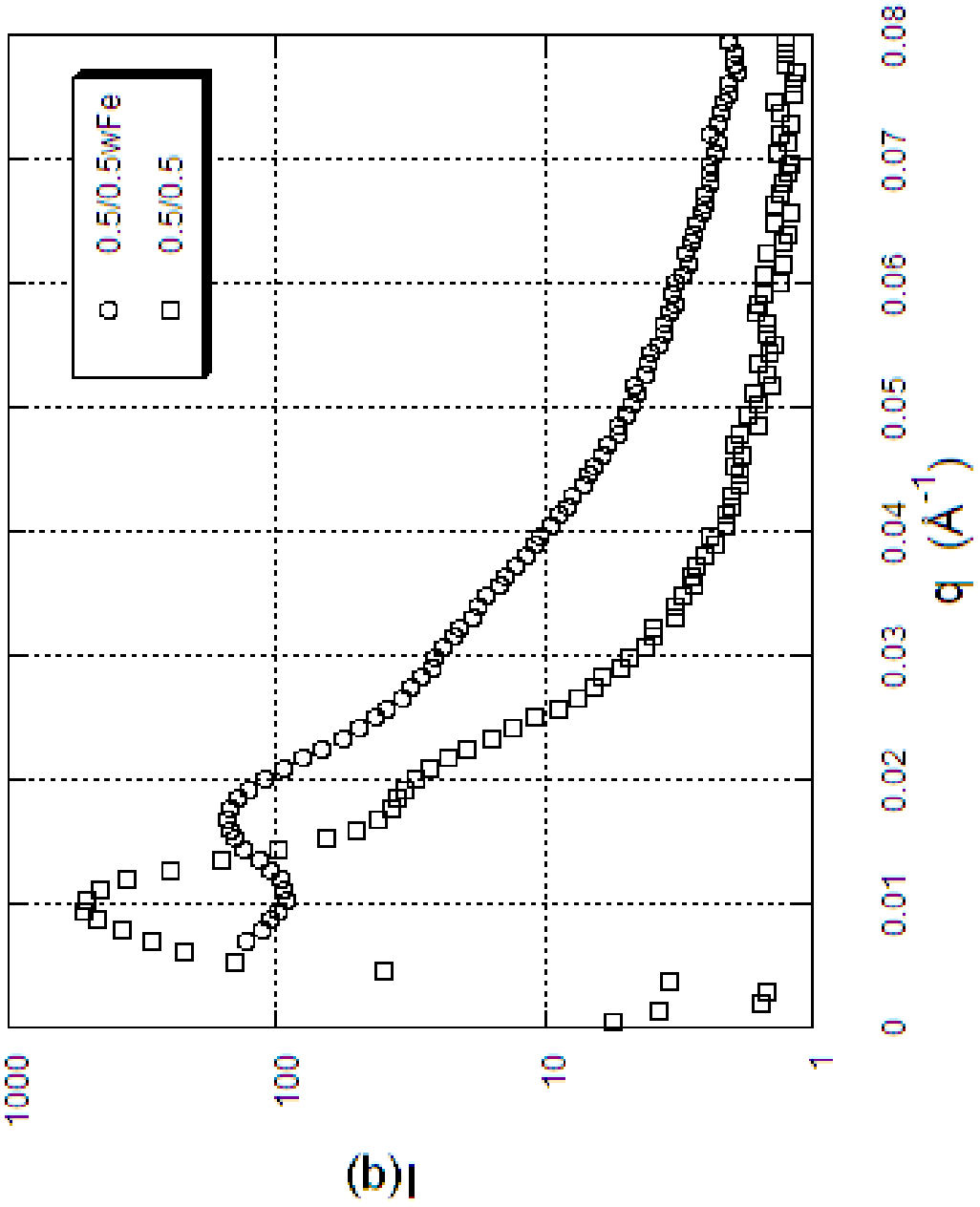

Figure 3.12: SANS profiles of the undoped and doped norbornene/deuterated norbornene dicarboxylic acid block copolymer with block ratios of 0.5/0.5. The doped sample contains 7 wt% Fe.

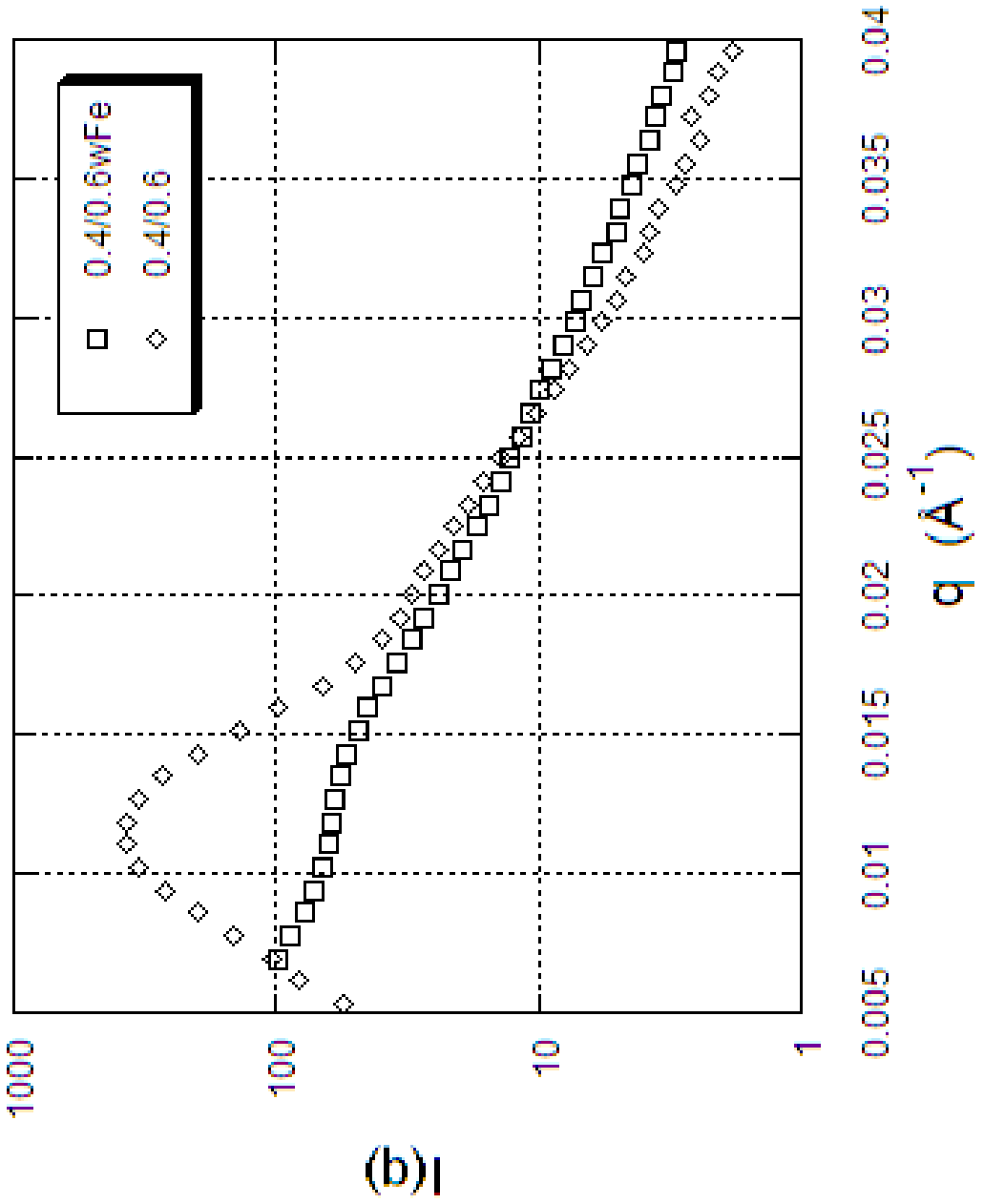

Figure 3.13: SANS profiles of the undoped and doped norbornene/deuterated norbornene dicarboxylic acid block copolymer with block ratios of 0.4/0.6. The doped sample contains 10 wt% Fe.

Transmission electron microscopy indicated that the diblock copolymers with Fe_2O_3 exhibited spherical and interconnected morphologies. The sample synthesized

with constituent block volume fraction ratio $\phi_{NOR/NORCOOH} = 0.64/0.36$ had a disordered spherical morphology with an average particle size of 10.4nm as shown in Figure 3.14. The spacing between the magnetic nanoparticles of this sample was determined by 2-dimensional Fourier transform (FFT) analysis of the TEM image. The spacing of the metal oxide particles, 62nm, was found to be close to the domain spacing of 53nm obtained by SANS. The comparison of I versus Q plots is presented in Figure 3.15.

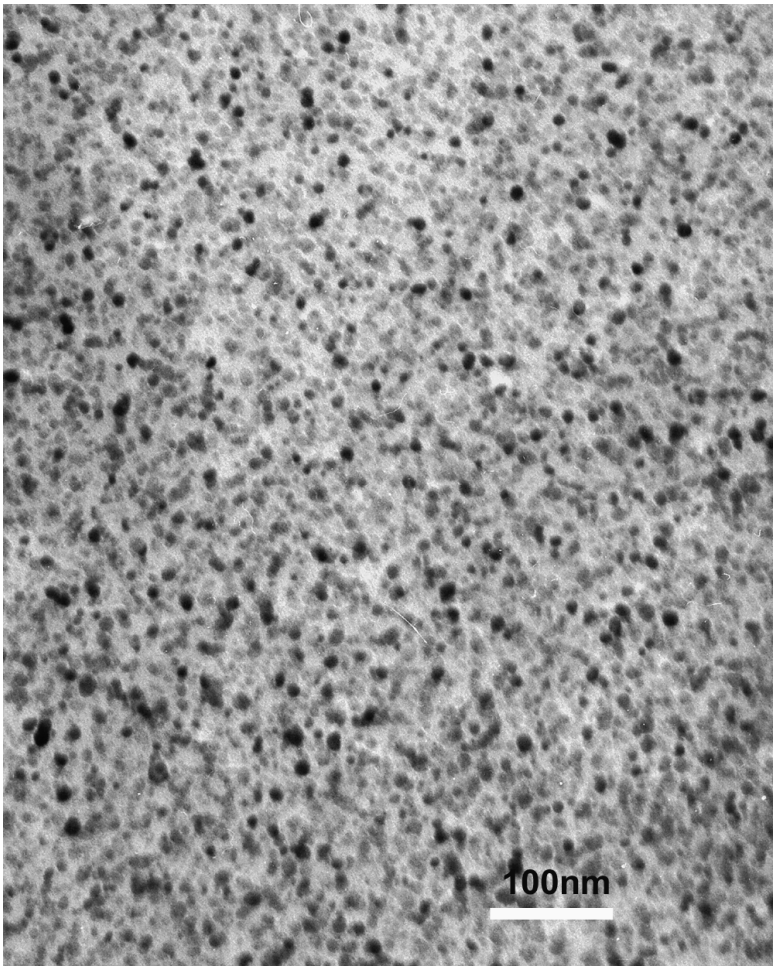

Figure 3.14: TEM image of 0.64/0.36 polymer doped with Fe_2O_3 nanoparticles.

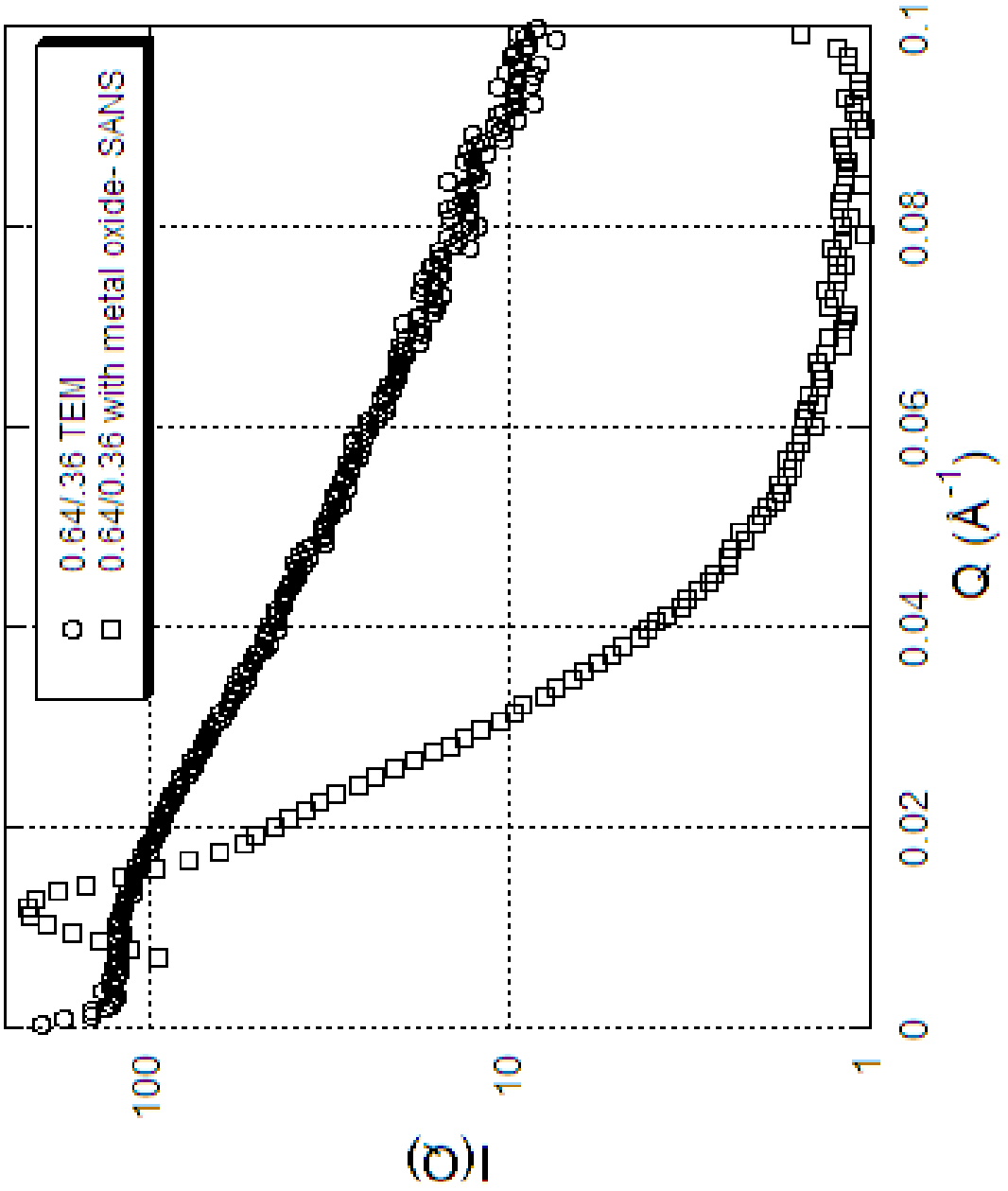

Figure 3.15: Comparison of d-spacings of metal oxide doped polymer 0.64/0.36 from SANS and TEM. The d-spacing between metal oxide nanoparticles and metal oxide doped polymer domains are found to be 62nm and 53nm, respectively.

The metal oxide doped polymer samples with 0.50/0.50 and 0.40/0.60 volume fraction ratios exhibited interconnected morphologies, as shown in Figures 3.16, 3.17.

The average particle size was found to be 10.7 and 16 nm for the sample with volume fractions of 0.50/0.50 and 0.40/0.60. The metal doped samples exhibit morphologies which were different than the expected morphologies from the original undoped copolymer compositions. The reason for the disordered morphologies can be the possible non-equilibrium conditions occurring during the solvent casting and the interparticle interactions affecting the microphase separation and desired morphology. For example, an interconnected morphology was observed from the diblock copolymer with 50/50 volume fraction ratio instead of the expected lamellar morphology. FFT of the TEM images did not give a peak for these samples because TEM images do not present enough order in the particular areas.

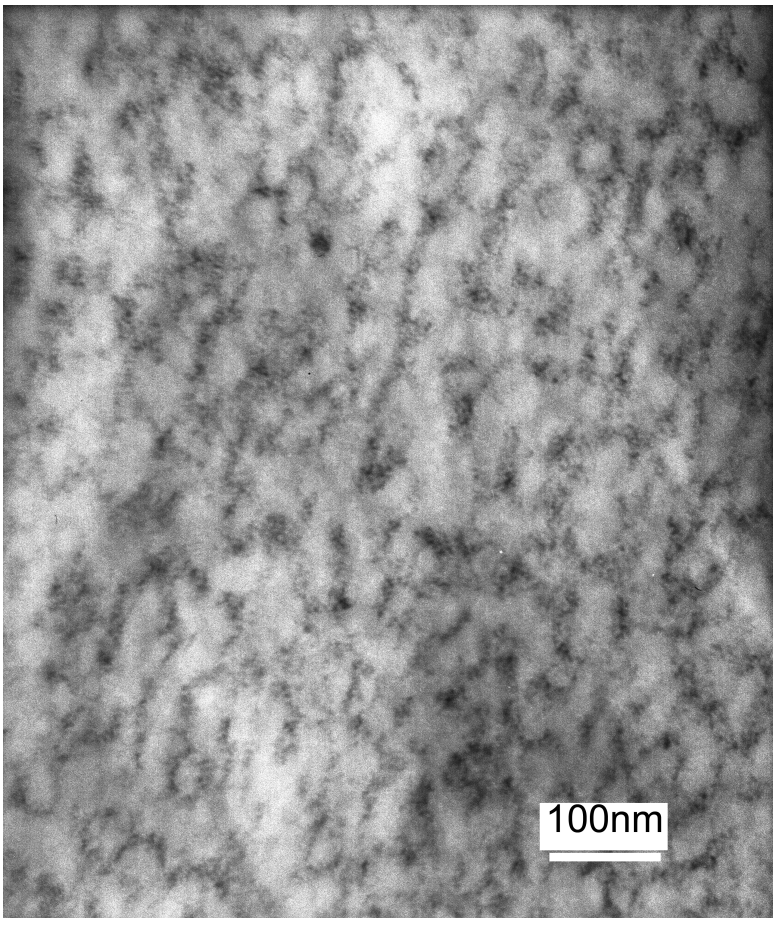

Figure 3.16: TEM image of 0.50/0.50 polymer doped with Fe_2O_3 nanoparticles.

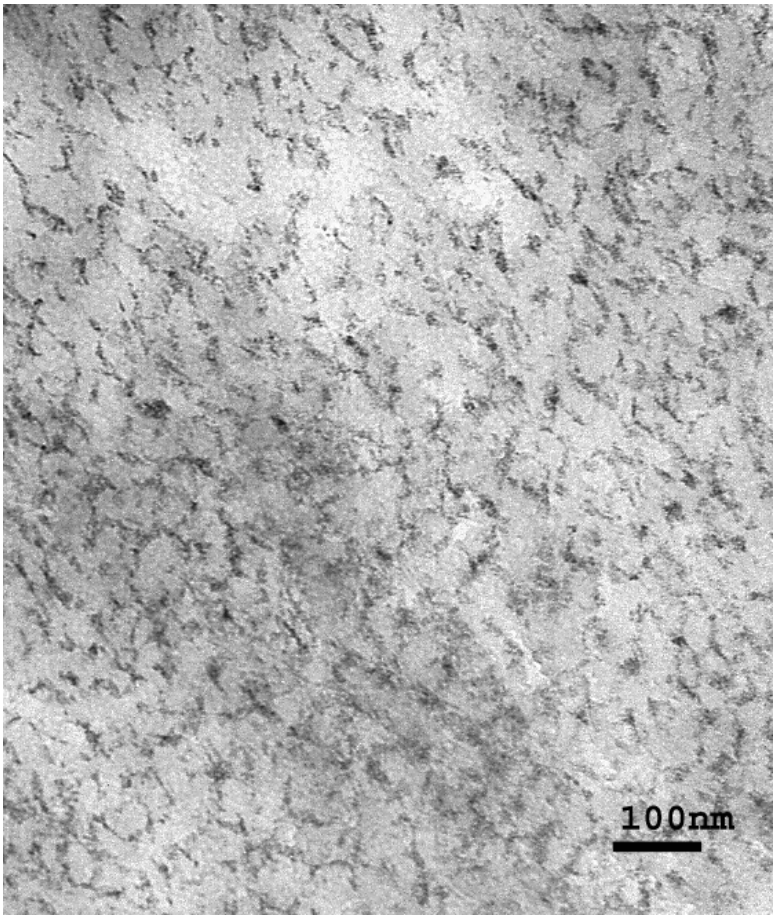

Figure 3.17: TEM image of 0.40/0.60 polymer doped with Fe_2O_3 nanoparticles.

3.3.3 Magnetic Characterization of Polymer-Metal Systems

All the ZFC curves shown in Figure 3.18 represent broad distributions of particle size and blocking temperatures. The blocking temperatures were calculated from the maxima of the ZFC curves.

The change in blocking temperature is related to the particle size and relaxation time distributions of the particles. The temperature T_s where the ZFC and FC curves meet, corresponds to the blocking of the largest particles. $T_s - T_b$ is a measure of the width of the energy barrier and thus relates to the particle size

distribution. Both temperatures, T_b and T_s are given in Table 3.10. In our study, it was found that the blocking temperature increased with decreasing polymer domain spacing. This behavior is probably related to interparticle interactions. Magnetic interactions between superparamagnetic particles may influence the relaxation time and anisotropy energy. The effect of particle interactions on the dynamic and static properties of γ-Fe_2O_3 nanoparticles dispersed in poly-vinyl alcohol homopolymer has been studied by ac susceptibility and Mossbauer spectroscopy measurements in an earlier study.[71] Thermal variation of the relaxation time has been observed for samples with different particle spacings. It was reported that as the ratio of center-to-center distance between particles (d) to average particle diameter (2R), $d/2R$, varied from 3.9 to 1.6, the energy barrier due to interactions ($E_B(0)$) increased from 38 to 275 and resulted in higher blocking temperatures.[51,72] Dormann et al. showed that the sample with the smallest particle spacing had the highest T_b within a series of samples with the same particle size. They found that the sample with d/2R$\sim$4.7 (which had the largest spacing) was consistent with noninteracting particles. The effect of relaxation of the particle moment on interparticle interaction energy was accounted for using a statistical calculation of the energy barrier. For our samples, the corresponding $d/2R$ ratios were determined to be 5.09, 3.50 and 2.29 for 0.64/0.36, 0.50/0.50, 0.40/0.60 samples, respectively. d values for the metal oxide doped polymers were determined from the SANS data and R was determined by TEM. These $(d)_{SANS}/(2R)_{TEM}$ ratios were similar in magnitude to the values found by Dormann et al. Therefore, the observed increase in T_b from 70K to 115K is probably due to the decreasing ratio d/2R and the concomitant increase in interparticle interactions.

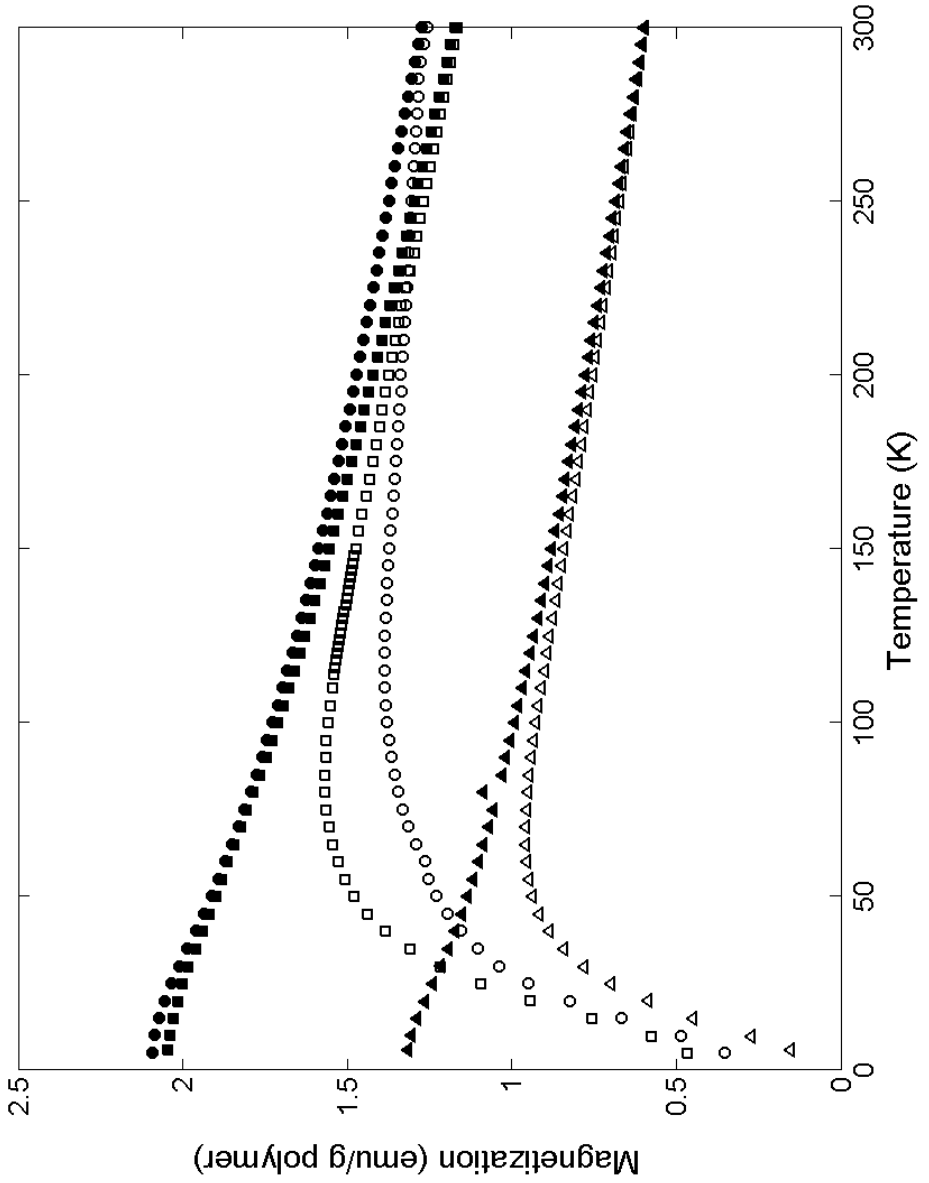

Figure 3.18: ZFC-FC magnetization curves as a function of temperature with 200 Oe applied magnetic field for sample 0.64/0.36(△), 0.50/0.50(□) and 0.40/0.60(∘). Filled and unfilled symbols represent FC and ZFC curves, respectively.

Polymer volume fractions	T_b, (K)	T_s, (K)	d/2R
0.64/0.36	70	200	5.09
0.50/0.50	85	250	3.50
0.40/0.60	115	290	2.29

Table 3.10: Blocking temperature variation with the block copolymer composition, obtained from ZFC measurements with SQUID.

The magnetizations at an applied field of 50 kOe per gram of polymer and per gram of Fe_2O_3 at different temperatures are presented in Table 3.11. Magnetization values increased with increasing amount of Fe_2O_3 in the diblock copolymers. The thermal dependence of magnetization was observed at 10, 50 and 300K between -0.5 kOe and 0.5 kOe. Magnetic measurements revealed that the samples were super-paramagnetic at room temperature. Below their blocking temperatures, hysteresis loops were observed for all samples. Figure 3.19 presents the magnetization profiles as a function of field for sample with volume fraction of 0.40/0.60 at 10K, 50K and 300K. Samples 0.64/0.36, 0.50/0.50 and 0.40/0.60 became ferrimagnetic at 10K. Magnetization profiles for all samples between -50 kOe and +50 kOe at 10K are presented in Figure 3.20. The magnetization of sample 0.40/0.60 with the highest metal oxide content remained unsaturated at the highest field 50 kOe, at 10K.

Polymer volume fractions	emu/g polymer		emu/g $\gamma - Fe_2O_3$	
	10K	300K	10K	300K
0.64/0.36	7	5	81	58
0.50/0.50	8	7	80	70
0.40/0.60	14	11	97	76

Table 3.11: Magnetization values at 50 kOe for varying block copolymer compositions at 10K and 300K.

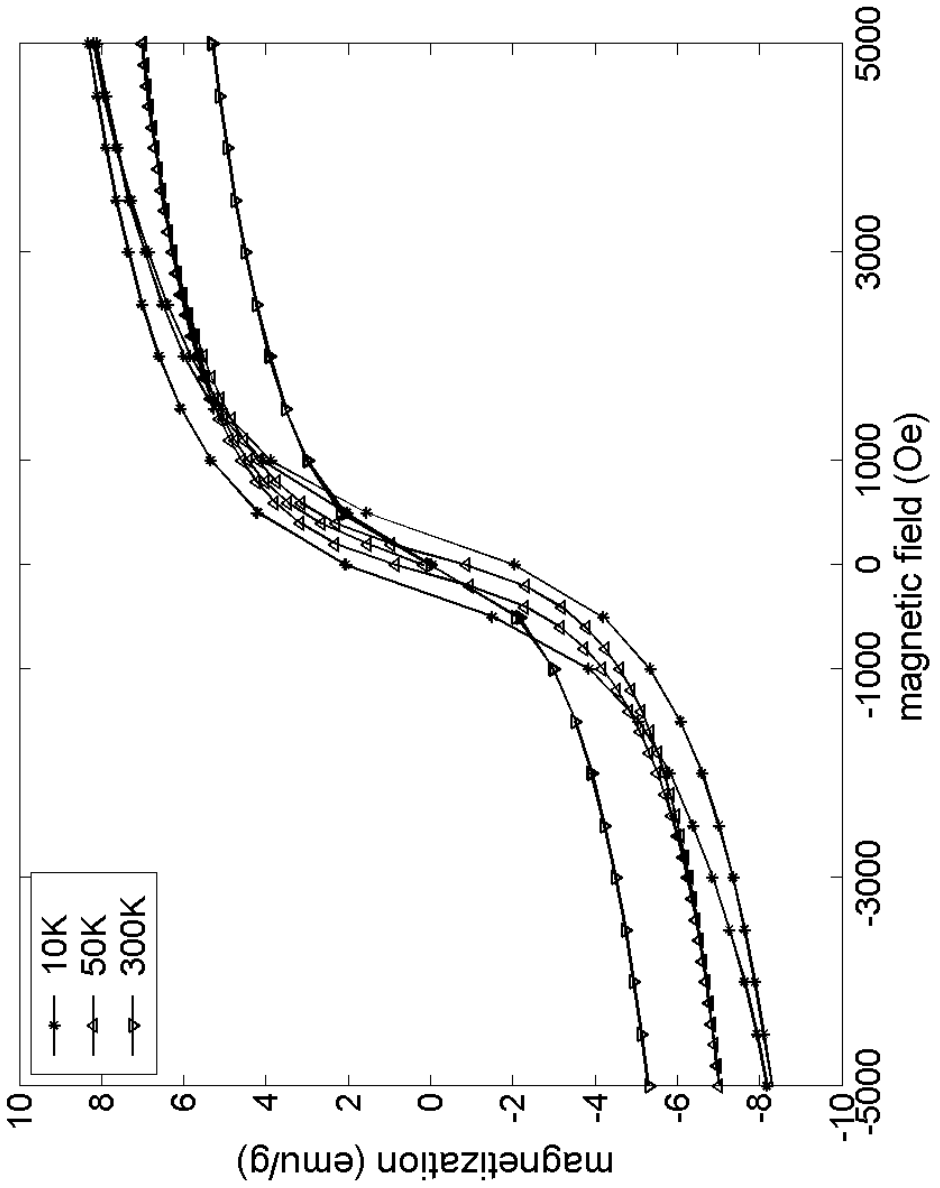

Figure 3.19: Magnetization versus applied magnetic field for the block copolymer with volume fraction of 0.40/0.60 containing Fe_2O_3 nanoparticles at 10K, 50K and 300K.

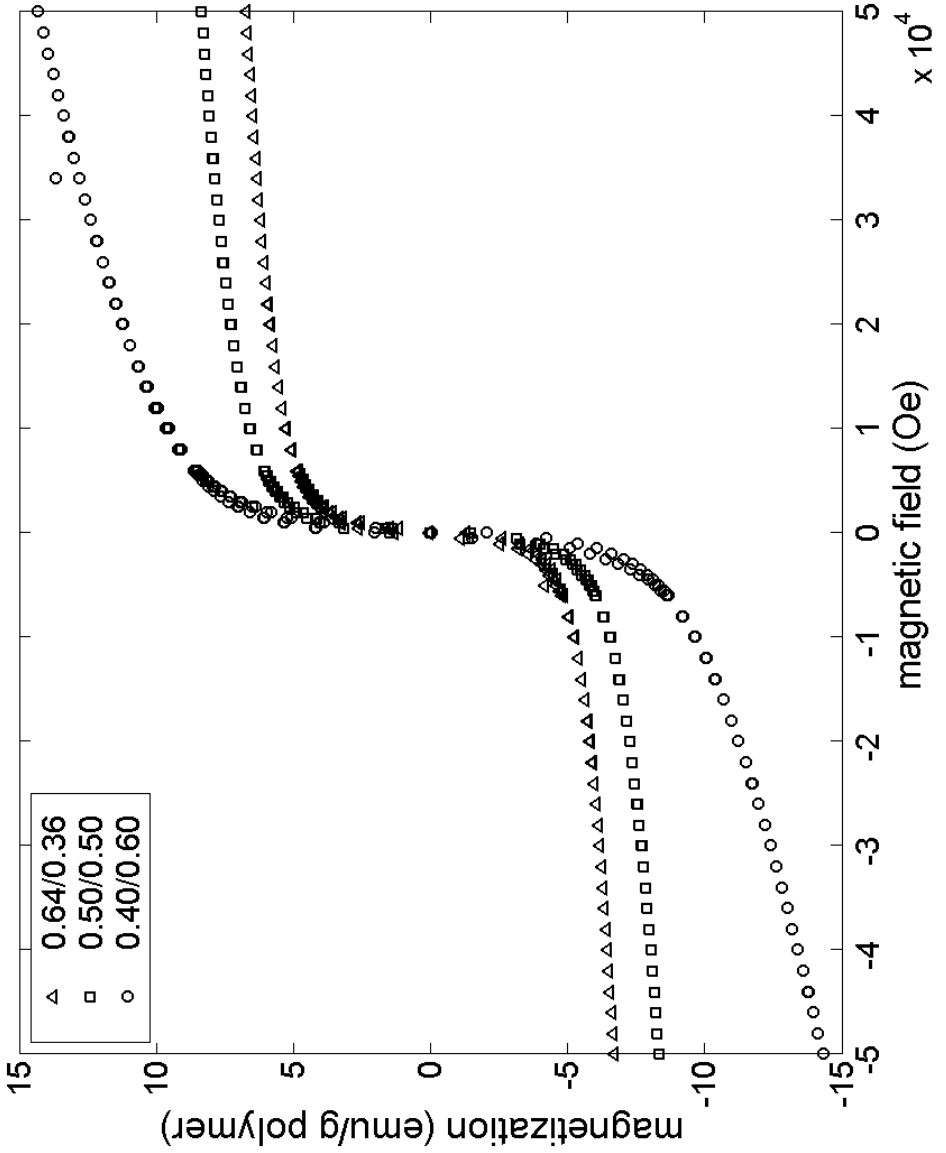

Figure 3.20: Magnetization versus applied magnetic field for all samples at 10K.

It was observed that the magnetization changed with block copolymer composition and increased with decreasing temperature for all the samples. Remanence values per gram of polymer at 10K are given for samples 360/120, 320/190 and

290/260 in Table 3.12. The remanence increased with decreasing temperature from 50K to 10K. With increasing Fe amount, the remanence and magnetization values increased.

Block copolymer composition	Remanence (emu/g)
360/120	1.29
320/190	1.48
290/260	2.06

Table 3.12: Remanence values per gram of polymer at 10K.

3.4 Conclusions

Spherical and interconnected morphologies of γ-Fe_2O_3 nanoparticles were synthesized within different copolymer structures and characterized in TEM. FFT analysis of the TEM image from the 0.64/0.36 sample showed that the spacing between the metal oxide particles in TEM image (62nm) was consistent with the polymer spacing of 53 nm measured by SANS. Similar spacings between polymer domains and metal oxide particles indicate the control on the dispersion of metal oxide particles within the diblock copolymer template.

The SANS profiles display significant changes in the shape and peak positions after metal doping. Nuclear scattering from magnetic particles can change the observed profiles if the iron particles are not distributed uniformly within the polymer nanodomains. Therefore, this change is due to non-uniform distribution of magnetic particles or their effect of strong dipolar interactions on the microphase separation of polymer domains. The effect of particle disordering and any change in polymer

structures is observed at high (10 wt%) Fe concentration.

High concentration of the nanoparticles may suppress the microphase separation of the copolymers due to the increasing effect of interparticle interactions of the aggregated particles. The relevant effect will be discussed in the following chapter. The amount of nanoparticles and their dispersion influence the interparticle interactions. Therefore the resultant magnetic behavior and properties of the metal oxide doped diblock copolymers may change.

An increase in blocking temperatures indicates particle interactions that change with particle size and domain distance. Sample (0.40/0.60) with the highest blocking temperature of 115K exhibited an interconnected morphology. All metal oxide doped samples exhibited superparamagnetic behavior at 300K and became ferrimagnetic at 10K.

The room temperature neutron scattering data does not contain spin-dependent magnetic scattering from Fe_2O_3 particles because all spins are disordered at this temperature. In order to distinguish the magnetic scattering, SANS experiments were performed at 10K. There was no change in the scattering profile at 10K when magnetic field of 5 Tesla was applied. The insignificant change in the scattering pattern under the applied fields was probably due to the spin disordering at the surface of the nanoparticles. Disordered spins present lower magnetization than that of the core spins and result in small magnetization at 10K. The unsaturation of magnetic spins at high fields was also indicative of the non-collinear behavior in all three samples. The magnetic property of the resultant spin structure was not sufficient to observe the magnetic ordering from the spins. Having disordered spin

structure on the shell can be difficult to align the spins at 5 Tesla and therefore any significant intensity increase in the scattering peaks and additional peaks could not be observed. Coey reported that even 5 Tesla was not sufficient to align all the spins of 6 nm γ-Fe_2O_3 particles.[52] Spin structure of the particles was suggested to be noncollinear due to competing antiferromagnetic exchange interactions at the surfaces of the particles. For small γ-Fe_2O_3 particles, spin-glass magnetic ordering (magnetically disordered surface layer) occurred near the surface of the particles.[46]

Chapter 4

Morphological Analysis of Undoped and Doped Poly(Norbornene)-block-Poly(Deuterated Norbornene Dicarboxylic Acid) Diblock Copolymers by TEM and SAXS

4.1 Introduction

The arrangement of inorganic nanoparticles within self-assembled diblock copolymers is the focus of many research investigations. Their extensive applications in electronics, magnetic and biotechnology have aroused the interest in understanding the arrangement of nanoparticles within organic or biological templates that aims to improve the performance of the molecular scale devices. As for templates, organic-organometallic block copolymers,[5] functionalized copolymers which have specific interactions with the nanoparticles[73] and micelles[33] have been utilized for the formation of ordered inorganic nanoparticle arrays.

We have been using norbornene based diblock copolymers as templates for the

synthesis of Fe_2O_3 nanoparticles. The Fe_2O_3 particles were selectively incorporated into the block containing carboxylic acid units which have strong interactions with the Fe^{+3} ions using a solution doping method,[74] and the spatial distribution of Fe_2O_3 nanoparticles and its influence on the magnetic properties of the nanocomposites were reported in previous chapter.

In this chapter, spherical, cylindrical and lamellar nanodomains of poly(norbornene)-b-poly(deuterated norbornene dicarboxylic acid) block copolymer were presented. Solution cast diblock copolymer bulk films were also investigated by means of Small-Angle X-ray Scattering (SAXS). The x-ray scattering profiles of the polymer samples displayed multiple high intensity peaks than those observed in neutron scattering measurements. The morphologies of norbornene based copolymers were examined by Transmission Electron Microscopy (TEM) through developing a new staining method. These self-assembled polymeric nanodomains were used as the templates for the synthesis of iron oxide nanoparticles. The doped copolymers were studied by SAXS. Analysis of the distribution of iron oxide nanoparticles within block copolymer templates and the undoped polymer morphologies revealed how well the nanoparticles were templated within the copolymer structures. The effect of Fe concentration on templating ordered particles was observed clearly. SAXS results also confirmed that by increasing the iron oxide doping concentrations, particles were arranged in a disordered manner. The influence of inorganic nanoparticles on the phase behavior of diblock copolymers has been studied theoretically by Balazs et al.[78] Their simulation results showed that depending on the particle volume fraction, the self-assembled structures can be changed. The disordered and connected iron

oxide structures that have been observed in norbornene based copolymers may also indicate the influence of high concentration of iron nanoparticles on the self-assembly and microphase separation of the block copolymers.

4.2 Characterization Techniques

Diblock copolymer morphologies were examined by TEM (Hitachi H-600, operated at 100keV). TEM samples were prepared by ultramicrotoming the solution cast undoped films using a Leica EM UC6 microtome with a diamond knife at room temperature. Undoped samples with longer NORCOOH blocks (samples with block ratios of 360/120 and 320/190 being the second block NORCOOH domain) were dry cut. The sample 375/60 was embedded in epoxy resin and thin sections (approximately 40nm) were microtomed. The undoped block copolymer morphology was observed after staining the microtomed sections with iodine vapor in a closed desiccator at room temperature for 6 hours.

Small angle x-ray scattering measurements before and after doping were carried out at beamline 12-ID-C (BESSRC) Argonne Research Laboratory, Advanced Photon Source (APS) at room temperature to observe the morphological differences between copolymers with different volume fractions.

4.3 Results and Discussion

NOR/d-NORCOOH copolymers with 0.2, 0.36, 0.50 and 0.62 volume fractions of d-NORCOOH were synthesized by ring-opening metathesis polymerization as dis-

cussed in Chapter 3. The block compositions, morphologies and the stoichiometric Fe amounts in the doped samples were shown in Table 4.1. Poly dispersity indeces for the correspondent samples were found to be 1.46, 1.67, 1.24 and 1.23, respectively from GPC/LS measurements. The multiple peaks observed in SAXS data indicate microphase separated and ordered structures of block copolymers at different compositions.

Volume Fraction ($\phi_{NORCOOH}$)	Morphology	Fe (wt%)
0.2	Spherical	4
0.36	Cylindrical	6
0.5	Cylindrical-lamellar	7
0.62	-	11

Table 4.1: Block ratios, volume fraction ($\phi_{NORCOOH}$), observed morphologies and the Fe amounts used in doped polymers.

The SAXS data of the doped samples correspond to the scattering from the metal particles due to the high electron density difference of the metal particles relative to the polymer matrix. The influence of the polymer template on nanoparticle arrangement is confirmed by comparing the SAXS plots of undoped and doped samples. Figure 4.1 shows the scattering curves of an undoped and metal oxide doped copolymer with a NORCOOH volume fraction of 0.2. The scattering peak at $0.00918\mathring{A}^{-1}$ indicates the microphase separation of the nanodomains with a d-spacing of $684\mathring{A}$. From elemental analysis, the iron amount was found to be 4 wt%. The major peak at $0.010577\mathring{A}^{-1}$ in the profile of polymer-metal sample indicates the spacing between iron oxide nanoparticles is $593\mathring{A}$. TEM image shows the spherical

microstructure of the undoped NOR/d-NORCOOH copolymer Figure 4.2. It was observed that norbornene domains were selectively stained by the absorbed iodine vapor, therefore the white dots represent the NORCOOH domains of the copolymer.

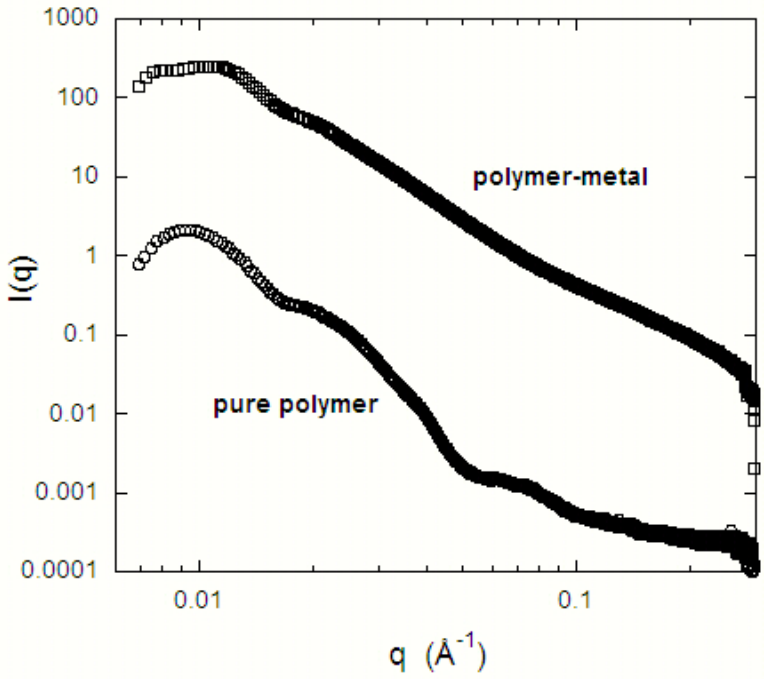

Figure 4.1: SAXS profiles of NOR/d-NORCOOH pure diblock copolymer and Fe_2O_3 doped polymer. The volume fraction of the NORCOOH block in the copolymer is 0.2. Metal oxide doped sample contains 4 wt% Fe.

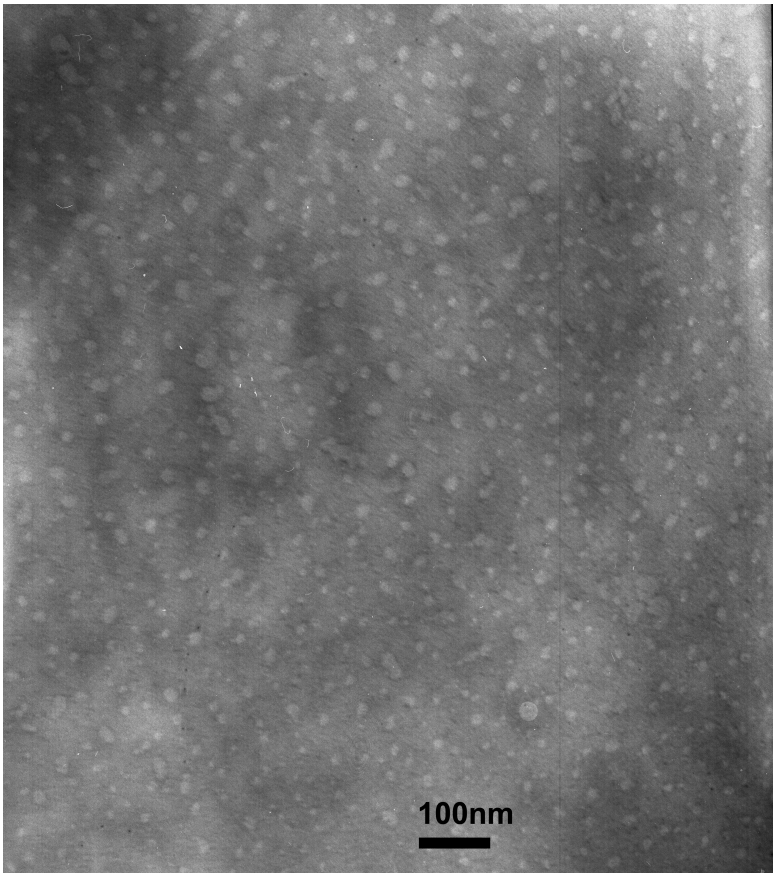

Figure 4.2: Electron micrograph of NOR/d-NORCOOH diblock copolymer with spherical morphology stained with iodine vapor. The volume fraction of the NOR-COOH block in the copolymer is 0.2.

The SAXS profile of the sample with NORCOOH volume fraction of 0.36 was measured at room temperature and the first order scattering maxima appeared at $0.010275\mathring{A}^{-1}$ while higher order scattering maxima of $\sqrt{3}$ and $\sqrt{9}$ were observed as shown in Figure 4.3. The relative positions of scattering maxima indicate a cylindrical domain structure. Electron microscopy of the undoped copolymer confirmed the cylindrical morphology after staining the microtomed sample (40nm thick film) with iodine vapor (see Figure 4.4). It was observed that most of the cylindrical microdomains in the solution cast film were oriented with the long axis parallel to

the film surface. The average center-to-center distance between cylindrical domains was calculated from the q value of the first peak as 61nm. The scattering profile of the doped copolymer indicates a disordered arrangement of the iron oxide particles within the cylindrical nanodomains when the particles were introduced by solution doping.

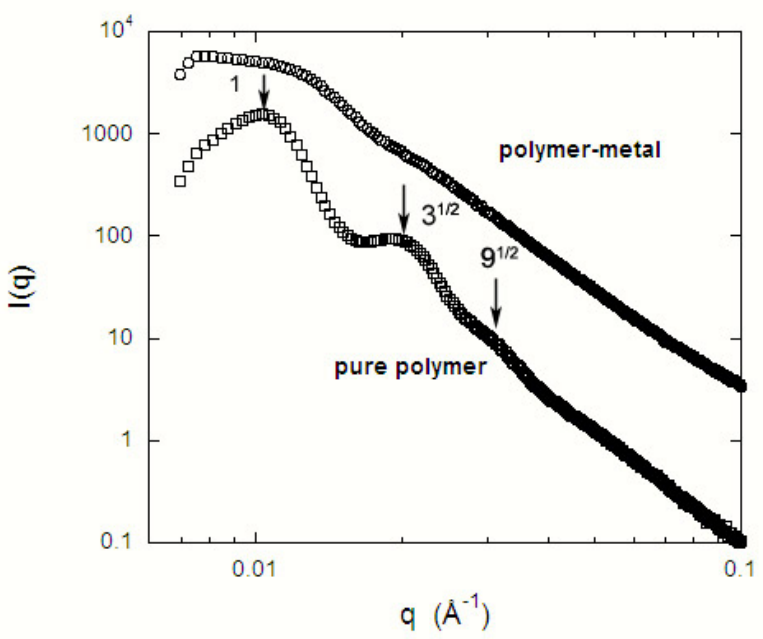

Figure 4.3: SAXS profiles of pure NOR/d-NORCOOH diblock and doped diblock copolymers. Volume fraction of the NORCOOH domain is 0.36. The Fe amount was found to be 6 wt% from elemental analysis.

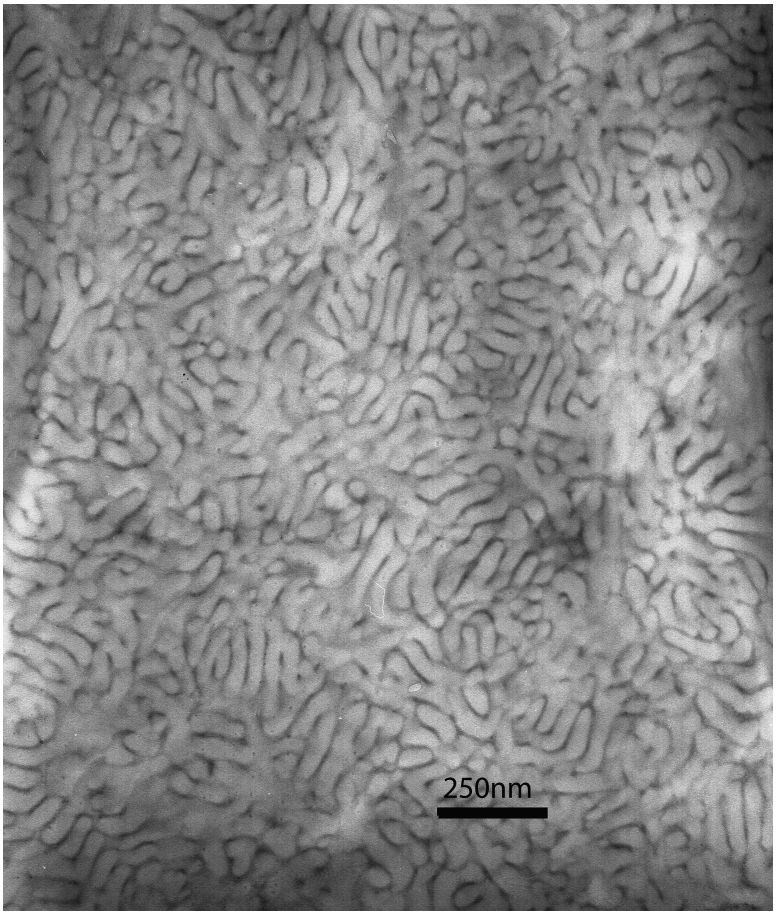

Figure 4.4: Electron micrograph of pure NOR/d-NORCOOH diblock copolymer with cylindrical morphology, stained with iodine vapor. Volume fraction of NORCOOH block is 0.36.

Figure 4.5 shows the cylindrical to lamellar morphology of the sample with the block ratio of 320/190 in which the volume fraction of the NORCOOH domain is 0.5. Hexagonal arrays of microdomains were oriented normal to the film surface at some parts of the film. Analysis of different parts of the film showed lamellar domains as depicted in Figure 4.6. NORCOOH volume fraction of 0.5 resulted in the cylindrical morphology mostly everywhere but also presenting lamellar domains which was expected for this composition. These morphologies present the non-

equilibrium structures. Samples were not annealed before analyzing in TEM. The Fe_2O_3 nanoparticle arrangement within this copolymer resulted in weakly ordered nanoparticles (Figure 4.7).

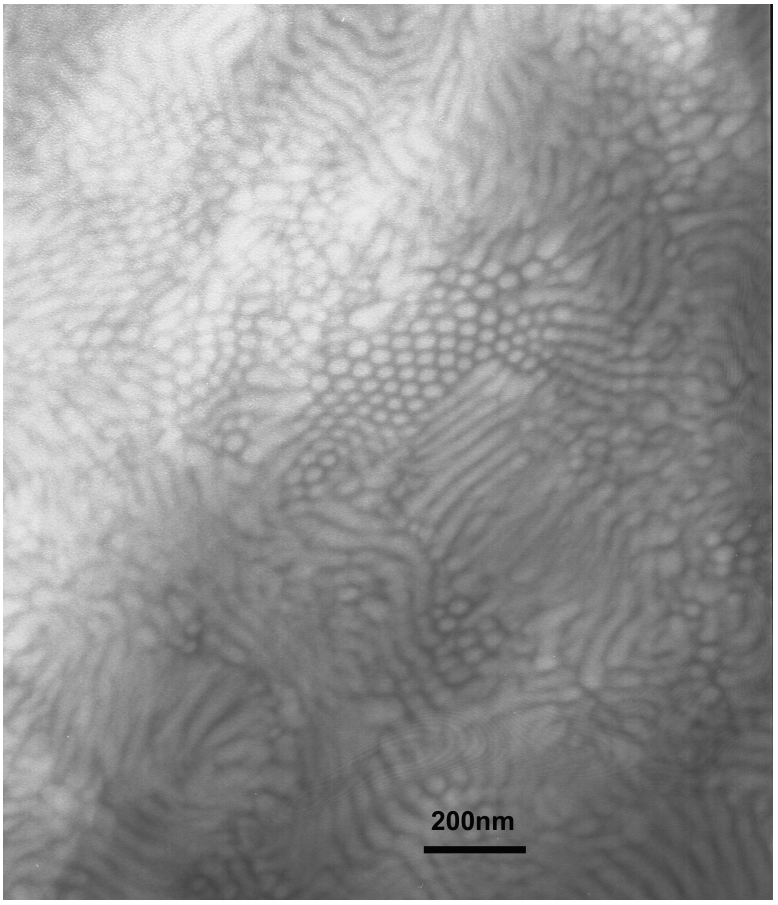

Figure 4.5: Electron micrograph of NOR/d-NORCOOH diblock copolymer with cylindrical morphology, stained with iodine vapor. Volume fraction of NORCOOH is 0.50.

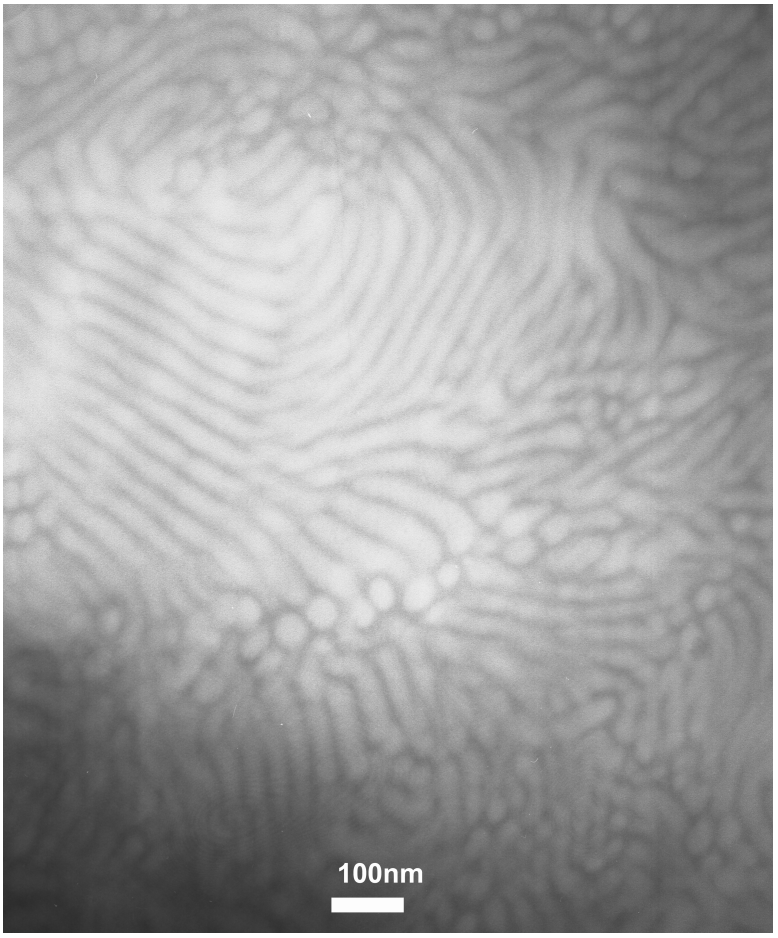

Figure 4.6: Electron micrograph of NOR/d-NORCOOH diblock copolymer with cylindrical to lamellar morphology, stained with iodine vapor. Volume fraction of NORCOOH is 0.50.

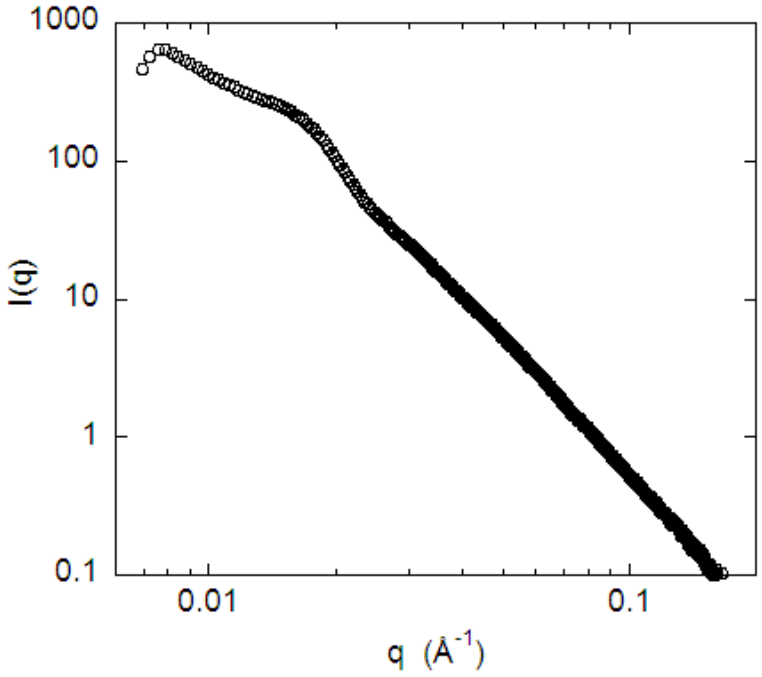

Figure 4.7: SAXS profile of Fe_2O_3 doped NOR/d-NORCOOH diblock copolymer. Volume fraction of the NORCOOH domain is 0.50. The iron amount was found to be 7 wt%.

The particles were disordered within the polymer with NORCOOH volume fraction of 0.62 even though the pure copolymer template was ordered which was indicated by the multiple scattering peaks (Figure 4.8).

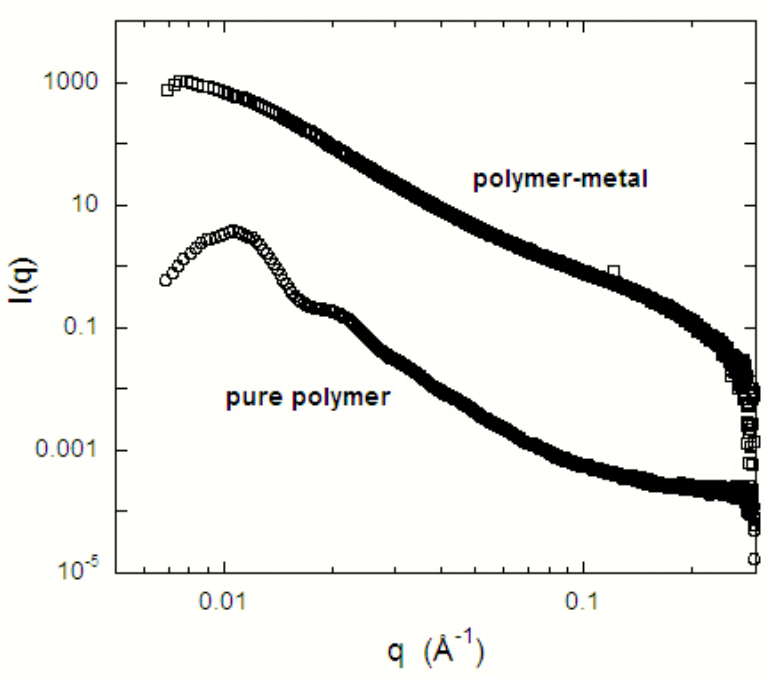

Figure 4.8: SAXS profiles of pure NOR/d-NORCOOH and Fe_2O_3 doped diblock copolymers. Volume fraction of the NORCOOH domain is 0.62. The iron amount was found to be 11 wt%.

By increasing the amount of Fe from 4 to 11 wt%, nanoparticles do not form ordered structures any more. The distribution of iron oxide particles was not uniform and disordered particles were observed when the iron concentration was increased to 11 wt% for the sample with block ratio of 304/297.

SAXS and TEM analysis of all undoped block copolymers verify that these polymers are microphase separated in spherical and cylindrical microstructures. It has been shown that the iron oxide distribution was not influenced by underlying copolymer morphology at increasing concentrations of Fe.

This result may indicate the potential influence on the microphase separation of copolymer when high concentration of Fe is added to the system. Hashimoto et

al. showed a similar result in PS-b-P2VP system containing palladium nanoparticles. Pd particles were produced by reduction of palladium acetylacetonate in dilute P2VP-b-PI solution. As the Pd particle concentration increased, free P2VP-b-PI blocks, which are responsible for formation of the well-defined microdomain structures, decreased in concentration.[75] In addition, free space between the Pd particles tend to decrease at high Pd concentration. Due to the interparticle interactions, the particles coordinated and stabilized by the polymer chains tend to form aggregates in which the P2VP may be segregated around the particles. As a result, high Pd particle content suppresses the microphase separated morphology and leads to interconnected aggregates.

It has been shown in earlier theoretical studies and simulations that the strength of interaction between the nanoparticles and the polymer domains affects the morphology of the copolymer mixture in melts. By tailoring the interaction energy between the particles and the one of the blocks, the structure and size of the domains has been controlled according to simulation results of Balazs et al.[76,77] In addition, the influence of inorganic particle size and concentration on the phase behaviour of diblock copolymers has been studied.[78]

4.4 Conclusions

Spherical, cylindrical and lamellar morphologies of poly(norbornene)-b-poly(deuterated norbornene dicarboxylic acid) block copolymers were visualized by TEM and the self-assembled nanostructures were examined in SAXS measurements. The morphological analysis of the influence of iron oxide nanoparticles embedded in poly(norbornene)-

b-poly(deuterated norbornene dicarboxylic acid) diblock copolymer was reported by SAXS and TEM of the doped samples. Exploring the morphologies of the undoped copolymers allowed us to determine the effect of templating mechanism which depends on the iron oxide particle amount. In conclusion, the distribution of Fe_2O_3 nanoparticles were controlled within NOR-b-NORCOOH copolymers when they were doped with low amounts of Fe (4 wt%), forming isolated spherical particles in the polymer template. High iron oxide particle concentrations (at 6 wt% and higher) were not templated within the microdomains of the copolymers. Thereby, at high concentrations of Fe, metal-metal particle interactions exceed the polymer-metal interactions resulting in the formation of disordered inorganic particles and disturbing the self-assembly of the diblock copolymer templates. At deformed copolymer morphologies due to high amounts of Fe, iron oxide particles aggregated forming interconnected nanoparticles. Theoretical studies of Balazs et al. also confirmed our results on the influence of high particle concentration on the evolution of a microphase separation.

Chapter 5

An Investigation of the Templating Fe_2O_3 Nanoparticles within Norbornene Methanol-Norbornene Dicarboxylic Acid Diblock Copolymers

5.1 Introduction

A novel diblock copolymer, poly(norbornene methanol)-b-poly(norbornene dicarboxylic acid), was synthesized at varying compositions and well dispersed iron oxide nanoparticles were synthesized within these polymer matrices. Norbornene methanol and norbornene dicarboxylic acid monomers have good solubilities in dichloromethane (CH_2Cl_2) in which the polymerization takes place. The synthesized sample with volume fraction of 0.5 for the norbornene methanol block displayed a lamellar morphology. Alternative doping on microphase separated thin films were employed. It was shown that the nanoparticles were aligned within the lamellar domains of the block copolymer when the thin film doping was applied. This re-

sult shows that diblock copolymers can be good templates for nanoparticle arrays when thin films were submerged in dilute iron salt solutions. On the other hand, transmission electron microscopy images of solution doped sample showed good dispersion of isolated and spherical iron oxide nanoparticles in diblock copolymers for the corresponding composition. The magnetic characteristics of these nanoparticles embedded in the copolymer matrix after solution doping results in ferrimagnetic behavior at 5K and high saturation magnetization per gram of polymer. The value is comparable to the bulk magnetization of Fe_2O_3 at low temperature.

In summary, the resulting nanoparticle morphologies from the two doping methods were examined with Transmission Electron Microscopy (TEM) and compared to the undoped copolymer morphology. Our results address the effect of polymer template and of the doping method on producing ordered metal oxide nanoparticles in thin and bulk films.

5.2 Materials

5-Norbornene-2-methanol (mixture of endo and exo) and 2-norbornene-5, 6, endo, exo-dicarboxylic acid, ethyl vinyl ether, dichloromethane (CH_2Cl_2), deuterated fumaric-2,3-D_2 acid (98 atom % D), bis(tricyclohexyl phosphine) benzylidine ruthenium(IV) dichloride (1st generation Grubbs' catalyst) and aqueous iodine solution (0.1M) (I_2) were purchased from Aldrich. CH_2Cl_2 was distilled over calcium hydride under argon. All solvents, monomers and catalyst required for polymer synthesis were stored inside an MBraun LabMaster100 glovebox.

5.3 Experimental

Methanol and carboxylic acid groups were protected by capping them with trimethylsilane. 5-trimethylsiloxylmethyl norbornene was synthesized as follows: 5-norbornene-2-methanol (8.25g, 0.0664 mole) and pyridine (5.25g, 0.0664mole) were stirred in 150ml ether under argon. Trimethylsilylchloride (7.21g, 0.064mole) was added slowly to the stirring solution. The solution was stirred under argon for 24 hour and filtered through celite. A second filtration was done through celite by washing with pentane. The liquid product was obtained after stripping the solvent and vacuum distilling it under 11.5 psi at 180°C. The distilled product was a clear, slightly viscous liquid and was kept in the glove box. The ^{1}H NMR spectrum of norbornene methanol (NORMeOH) is shown in Figure 5.1. As seen in Figure 5.2, two doublets of methylene protons which were identified at 3.24 and 3.38 ppm disappeared after methanol groups were capped with trimethylsilane. The chemical shifts of the NMR spectra are presented in Table 5.1.

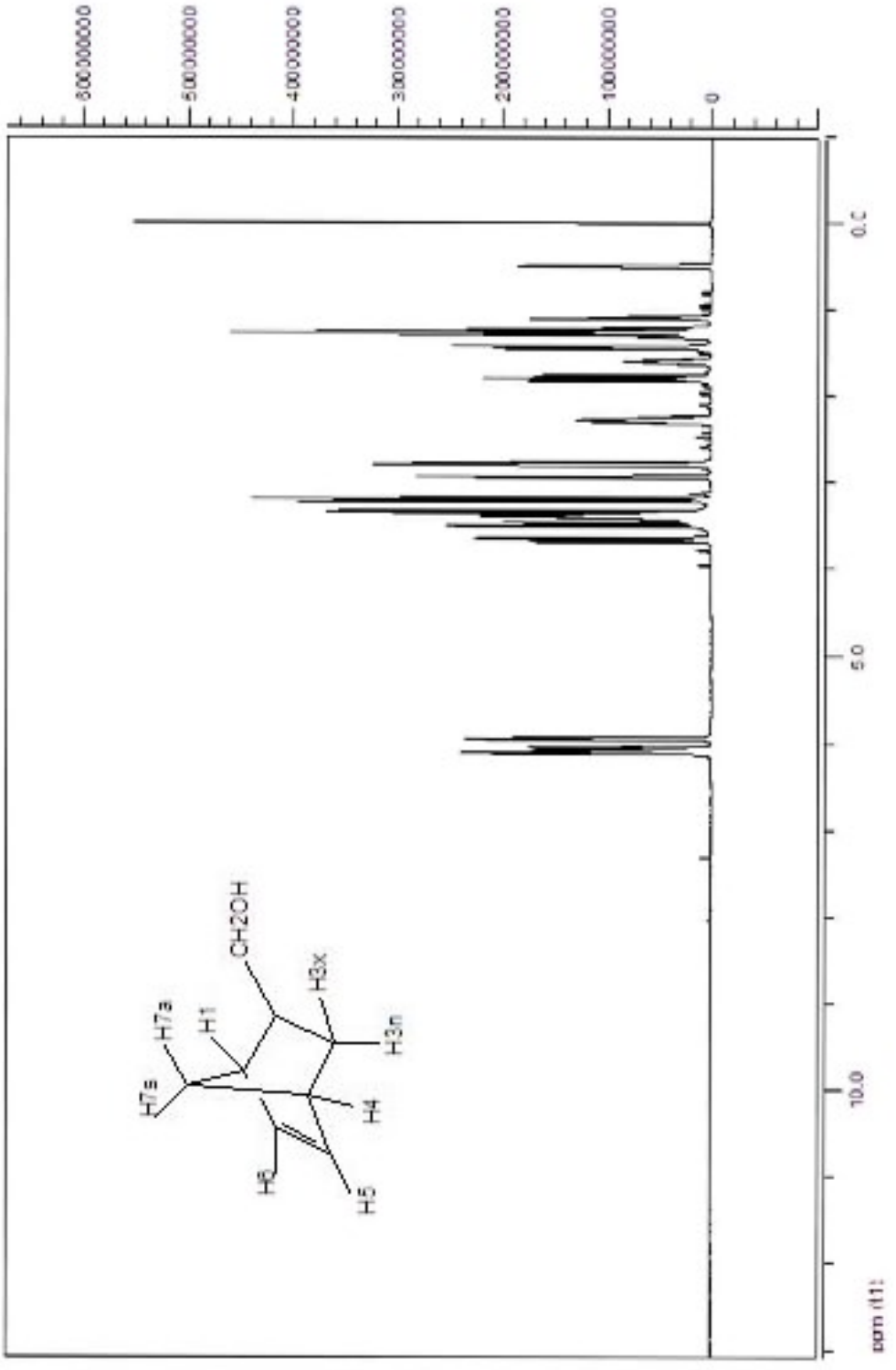

Figure 5.1: ^{1}H NMR spectrum of NORMeOH.

Positions	^{1}H Chemical Shifts (ppm)
H1	2.93 (endo), 2.75 (exo)
H2	2.29 (endo), 1.61(exo)
H3x	1.80(endo), 1.09 (exo)
H3n	0.49 (endo), 1.23 (exo)
H4	2.79 (endo), 2.81 (exo)
H5	6.12 (endo), 6.06(exo)
H6	5.95 (endo), 6.09 (exo)
H7s	1.43 (endo), 1.31 (exo)
H7a	1.25 (endo), 1.28 (exo)
CH_2OH	3.24, 3.38 (endo), 3.43, 3.60 (exo)

Table 5.1: ^{1}H Chemical shifts of the NMR of 2,5 endo-/exo-norbornene methanol.

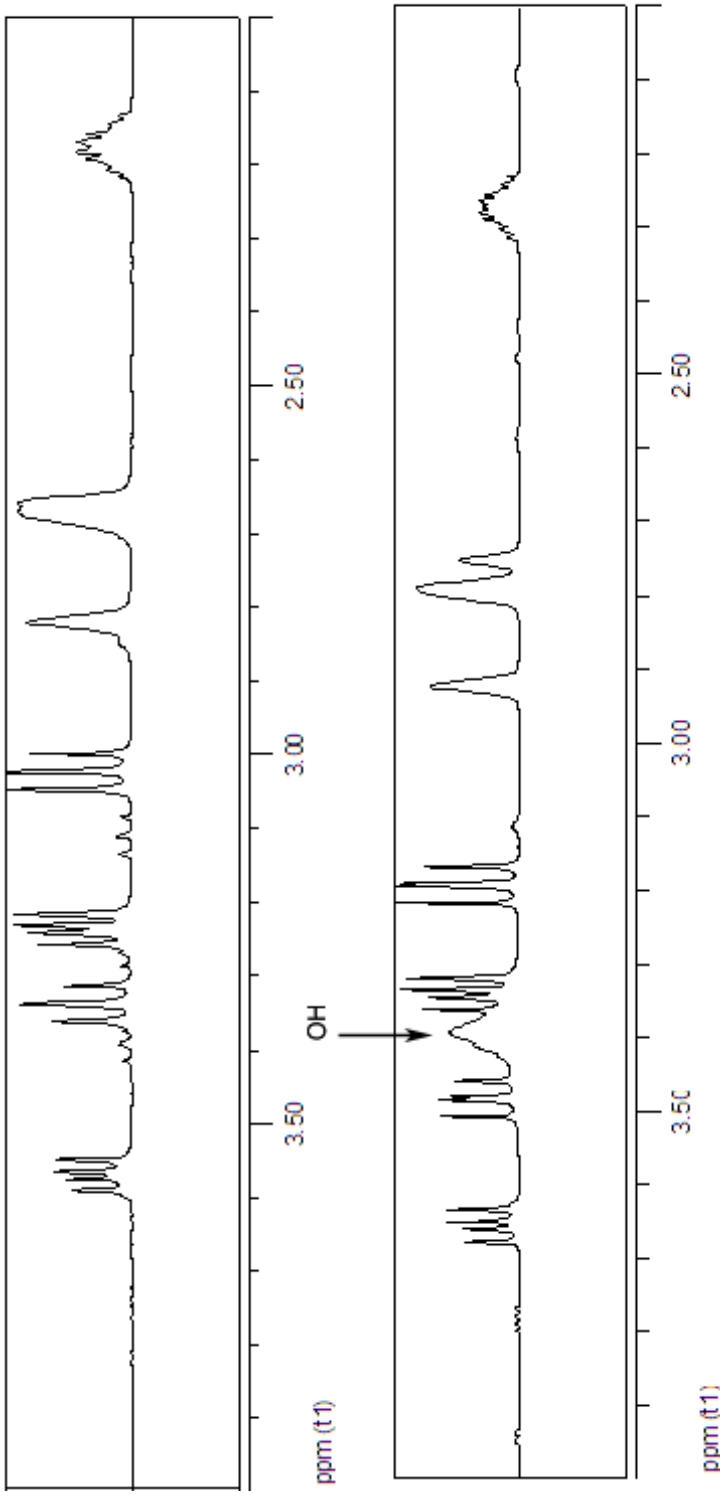

Figure 5.2: ^{1}H NMR spectrums of NORMeOH and NORMeOH-TMS.

2-norbornene-5,6 dicarboxylic acid bis(trimethylsilyl) ester was synthesized as reported in literature.[79] The norbornene methanol (NORMEOH)-norbornene dicarboxylic acid (NORCOOH) diblock was synthesized using Grubbs' catalyst in CH_2Cl_2 by first initiating the norbornene methanol trimethylsilane monomer. Polymerization of 5-trimethylsiloxylmethyl norbornene took 24 hours and 2-norbornene-5,6 dicarboxylic acid bis(trimethylsilyl) ester was added and stirred for another 24 hours. The reaction was terminated with ethyl vinyl ether and the diluted polymer solution was stirred with alumina to remove the catalyst. The polymerization mechanism is shown in Figure 5.3.

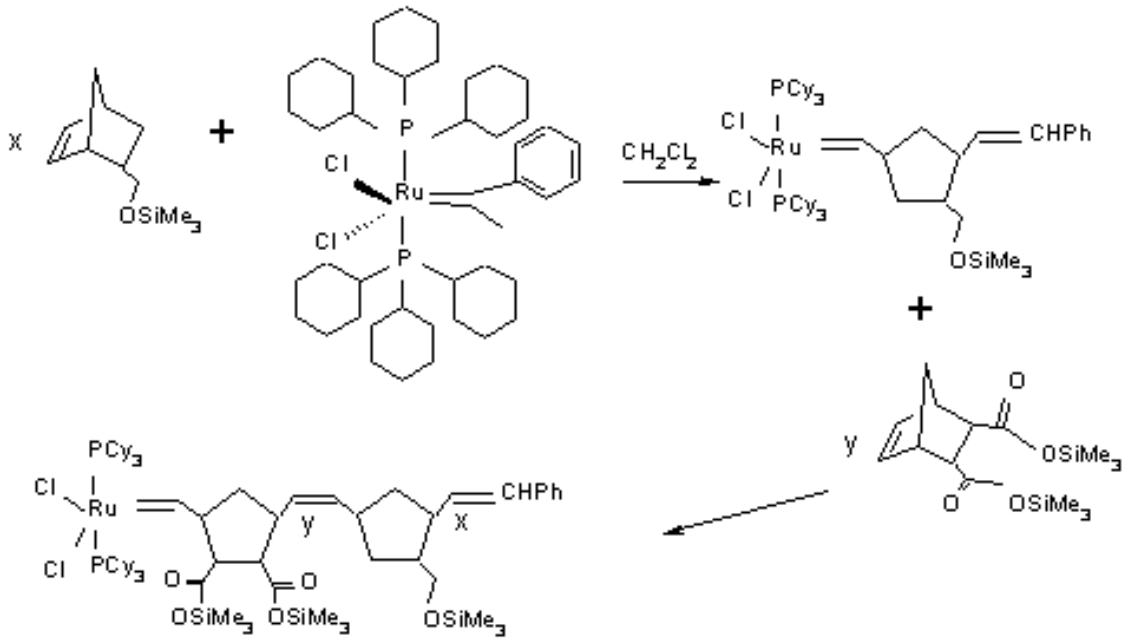

Figure 5.3: Polymerization schematic of NORMEOH-NORCOOH diblock copolymer.

5.4 Results and Discussion

The PDIs of the synthesized block copolymers were determined by Gel Permeation Chromatography - Light Scattering (GPC-LS). Target block ratios of NORMEOH-NORCOOH diblock copolymer and their PDI values are shown in Table 5.2. The actual molecular weights of the copolymers could not be determined due to unknown values of the exact sample concentrations and their $\frac{dn}{dc}$ values. The methanol and carboxylic acid groups were hydrolyzed by adding 0.5ml acetic acid to remove the trimethylsilyl protecting groups through rigorous stirring in air and then films of diblock copolymers were slowly static cast for 5 days under a CH_2Cl_2 saturated atmosphere in a dessicator.

Sample block ratio (NORMEOH/NORCOOH)	PDI
50/50	1.12
60/40	1.25
10/90	1.12

Table 5.2: Polydispersity indices of NORMEOH/NORCOOH diblock copolymer of actual block ratios as determined by UV spectroscopy.

The polymer compositions were determined using Perkin Elmer Lambda 25 UV-VIS spectroscopy. A calibration curve was obtained by measuring the absorbance as a function of the volume fraction of NORMEOH homopolymer in a series of NORMEOH and NORCOOH homopolymer blends. A sweep run was performed between wavelengths 210-310 $\mathring{A}$. As norbornene methanol fraction increased in the mixture, the intensity of the peak between 225-250 $\mathring{A}$ increased. The pure norbornene methanol homopolymer showed a peak maximum at 239 $\mathring{A}$. The absorbance values at 239 $\mathring{A}$ were monitored for samples with varying norbornene methanol amount. A calibration curve was formed by plotting the absorbance values at 239 $\mathring{A}$ as a function of norbornene methanol volume fraction (Figure 5.4). NORMEOH/NORCOOH diblock copolymer with 0.4 volume fraction of NORMEOH was microtomed and immersed in 4% aqueous OsO_4 solution for 12 hours at room temperature and then rinsed with water. The undoped morphology of the copolymer was seen in Figure 5.5.

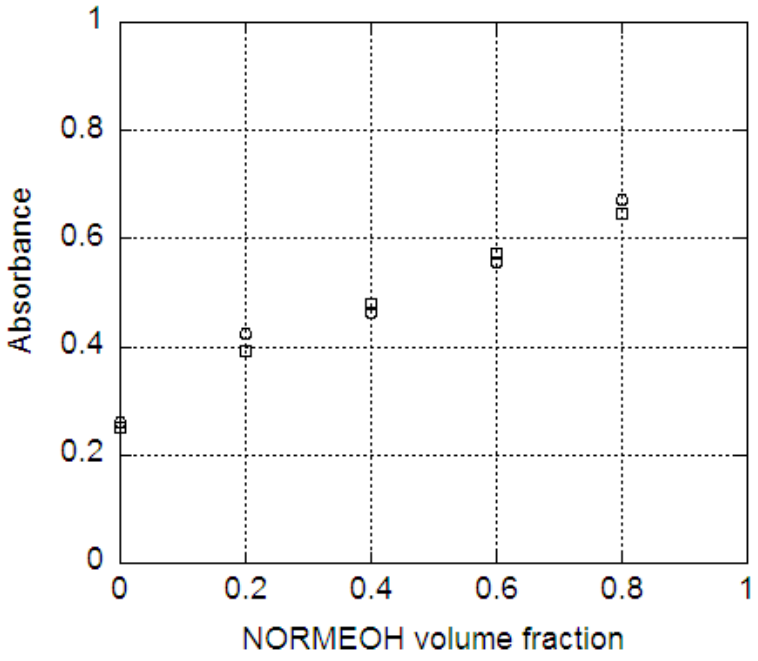

Figure 5.4: Calibration curve showing the absorbance change as a function of volume fraction of NORMEOH homopolymer in NORMEOH/NORCOOH mixtures.

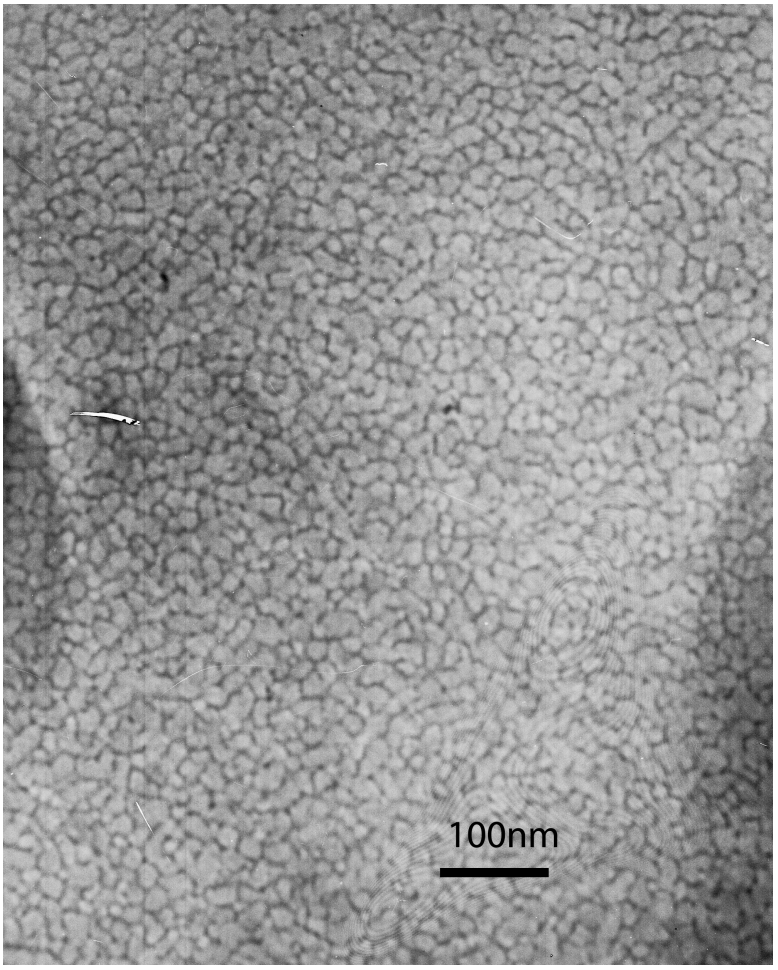

Figure 5.5: Electron micrograph of NORMEOH/NORCOOH diblock copolymer with 0.4 volume fraction of NORMEOH block, stained with OsO_4.

The iron particles of 3-5 nm in diameter were templated within this sample of NORMEOH/NORCOOH diblock copolymer after solution doping as shown in Figure 5.6.

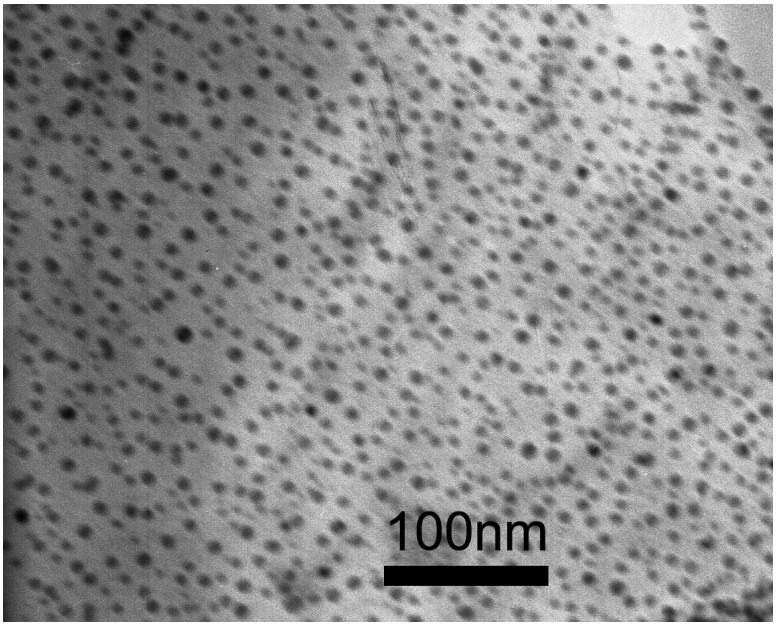

Figure 5.6: Electron micrograph of NORMEOH/NORCOOH diblock copolymer with 0.4 volume fraction of NORMEOH block, doped with Fe_2O_3.

Well dispersed iron oxide nanoparticles within norbornene methanol-norbornene dicarboxylic acid diblock copolymers were synthesized. These nanoparticles were superparamagnetic at room temperature. At 5K, the sample was ferrimagnetic and magnetic moments of 11 emu/g polymer was observed at 5 Tesla as shown in Figure 5.7. This copolymer contains 15.4 wt% Fe_2O_3 and its magnetization corresponds to 73emu/γ-Fe_2O_3 which is very close to the saturation magnetization of bulk γ-Fe_2O_3 (M_s=82emu/g at 5K). The hysteresis loop corresponded to a coercivity of 200 Oe and remanence of 0.68emu/g polymer at 5K. We believe that the better ordering and size uniformity of iron oxide nanoparticles resulted in a high magnetic moment and coercivity within this polymer matrix.

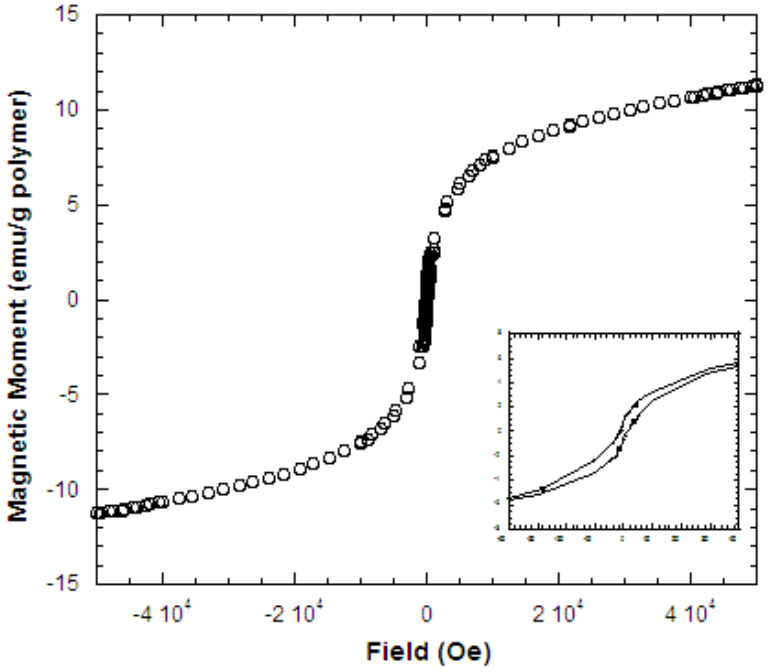

Figure 5.7: Magnetization versus applied field measured at 5K. The inside picture presents M-H profile between -4000/4000 Oe.

Figure 5.8 shows the distribution of spherical iron oxide nanoparticles in another sample which has the volume fraction of the NORMEOH block as 0.1.

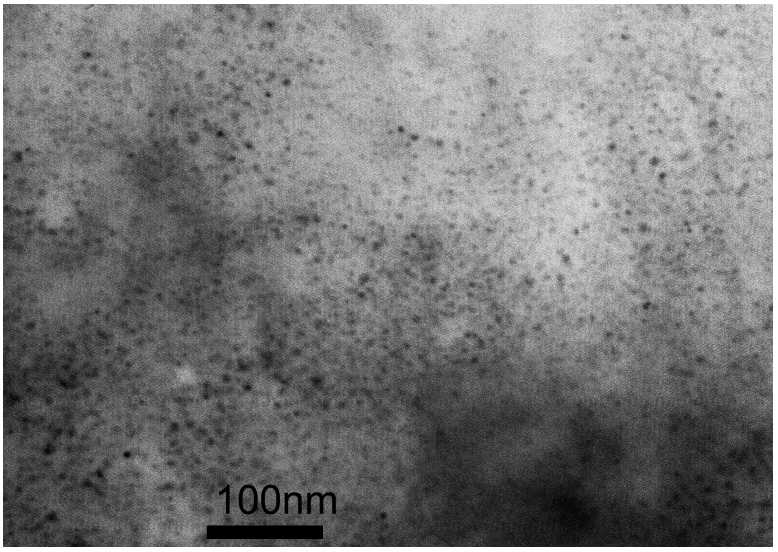

Figure 5.8: Electron micrograph of NORMEOH/NORCOOH diblock copolymer ($\phi_{NORCOOH}$=0.1), doped with Fe_2O_3.

Electron microscopy images of the doped samples showed that by loading the polymers with the stoichiometric amount of $FeCl_3$ in solution, the resultant nanoparticle arrangement was not controlled with the polymer template. For the sample containing 0.5 volume fraction of NORMEOH block, we employed an alternative doping method and compared the obtained microstructures with the undoped copolymer morphology. In the following sections, the staining, doping methods and TEM images are discussed.

5.4.1 Staining Diblock Copolymer:

Samples for TEM analysis were prepared by ultramicrotoming the solution cast undoped and metal oxide doped films. Films were embedded in epoxy resin and thin sections (approximately 40nm) were obtained by microtoming using a Leica EM UC6 microtome at room temperature with a diamond knife. The microtomed

sections were put on microscope slides and placed in a dessicator containing aqueous iodine solution. The samples were stained by exposure to iodine vapor for 6 hours. Iodine staining was achieved by the differential physical sorption of iodine into one of the blocks.

5.4.2 Metal Loading Methods:

Two metal loading methods (thin film versus solution) were employed to examine the effect of the doping process on the particle dispersion. In thin film doping, iron oxide particles were associated to the carboxylic groups of a thin film (approximately 40nm thick) that was prepared by microtoming. The microtomed sections were soaked in 0.007M NaOH solution for 16 hours, rinsed with water and then immersed in 5mM aqueous $FeCl_3$ solution for 5 minutes.[61] In this method, Fe^{+3} ions exchange directly with the Na^{+1} ions associated to the COOH group leading to a faster iron ion uptake within the thin film.

The solution doping procedure was followed as stated in literature.[3,18] The block copolymer solution (5 wt%) was mixed with a $FeCl_3$ solution in tetrahydofuran under argon for 12 hours. The polymer-metal solution was cast in solvent saturated atmosphere to form bulk films. The films were soaked in 2M NaOH solutions to produce Fe_2O_3 particles for 24 hours. A final water wash removes any unbound metal and sodium salts. It is known that the solution doping mechanism followed by oxidation produces well dispersed but disordered γ-Fe_2O_3 nanoparticles within the block copolymer matrix.[74] These iron oxide doped films were embedded in epoxy resin and then microtomed into 40 nm thick sections. The morphologies

of the undoped and doped copolymers were examined using TEM (Hitachi H-600, operated at 100 keV).

In previous studies, the morphology of norbornene based diblock copolymers has been reported in two systems: A norbornene dicarboxylic acid-b-acetylene diblock copolymer, stained with diethyl zinc vapor[79] and norbornene methanol-b-carbazole functionalized norbornene stained with dimethyl cadmium ($Cd(CH_3)_2$) vapor.[80] After vapor staining, these block copolymers were microtomed into thin sections for TEM characterization. The solution and thin film metal oxide doping methods have been applied to many block copolymer/nanoparticle systems by Cohen et al.[3,15,16,18,61] However, the morphologies obtained using different doping methods have not been compared to the undoped copolymer in the same polymer system.

The TEM of the undoped norbornene methanol/norbornene dicarboxylic acid diblock copolymer which was ultramicrotomed and then stained with iodine displayed a lamellar morphology as shown in Figure 5.9. Lines with different thicknesses probably formed from the segregated silane groups which were used for protecting the functional groups on both blocks. From this figure a domain spacing of 50nm (measured between the two dark lines) was calculated. The fast fourier transform (FFT) image of the corresponding electron micrograph shows the diffraction pattern of the lamellar domains as displayed in the insert of Figure 5.9.

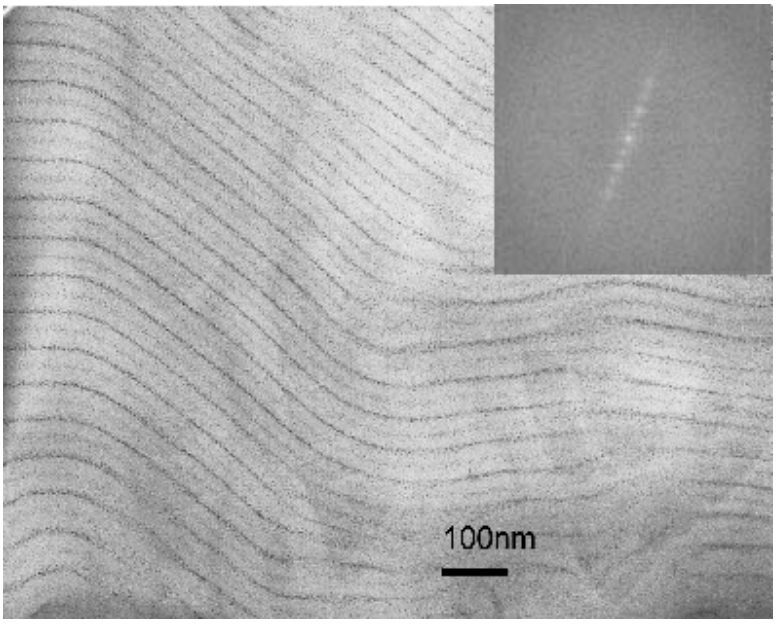

Figure 5.9: Electron micrograph of NORMEOH/NORCOOH diblock copolymer, stained with iodine vapor. The inside picture shows the FFT image.

The thin film metal oxide doping method was employed to microtomed sections of the block copolymer sample. The ordering of the iron oxide nanoparticles followed the lamellar morphology of the pure copolymer as indicated by the TEM micrograph of Figure 5.10. The $\gamma - Fe_2O_3$ nanoparticles were lined up along one of the individual lamellar domains and the distance calculated between two adjacent nanoparticle arrays was between 70 to 90 nm. However, the diblock copolymer doped using the solution method resulted in interconnected aggregates of iron oxide nanoparticles (Figure 5.11) which were not templated by the underlying block copolymer structure.

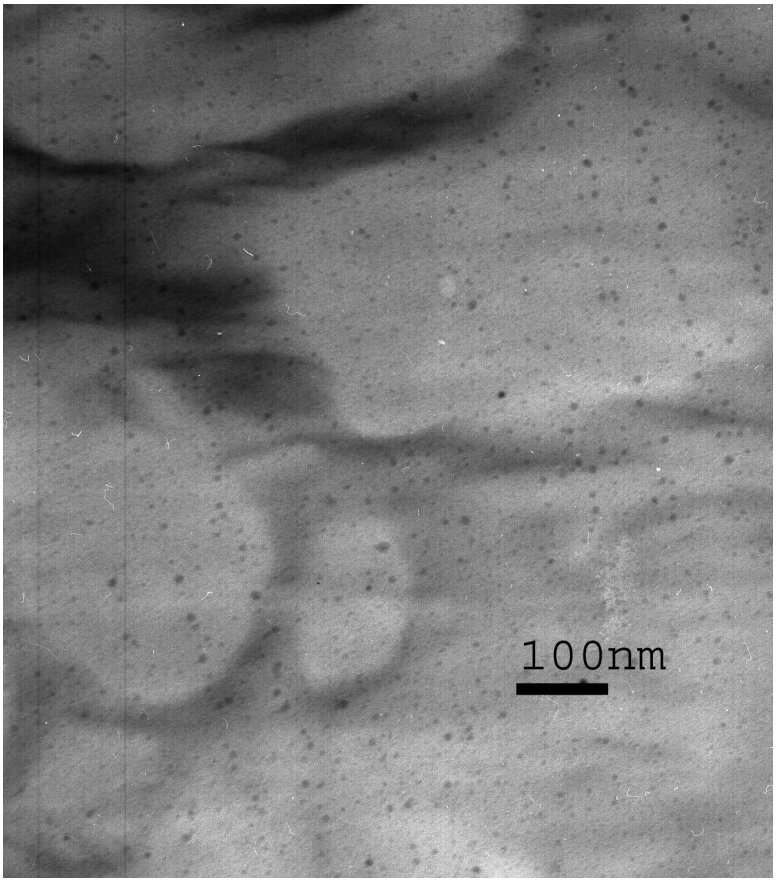

Figure 5.10: Electron micrograph of the iron oxide doped NORMEOH/NORCOOH diblock copolymer. Sample was prepared by submerging a thin film in $FeCl_3$ solution (thin film doping).

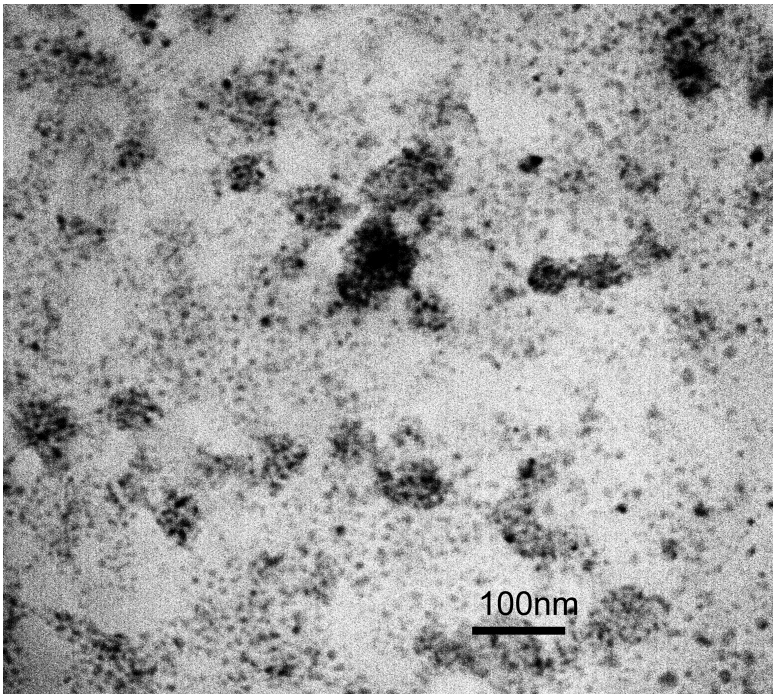

Figure 5.11: Electron micrograph of the iron oxide doped NORMEOH/NORCOOH copolymer prepared by solution doping.

The main difference between the two metal oxide doping methods is that in the thin-film doping case, the block copolymer microphase separation has occurred prior to metal doping. The pre-existing lamellar microstructure guides the preferential binding and confinement of $\gamma - Fe_2O_3$ within the carboxylic acid containing polymer block.

5.5 Conclusions

We have synthesized norbornene methanol/norbornene dicarboxylic acid diblock copolymers with low polydispersity indices. Polymers doped with iron ions in solution did not form ordered iron oxide nanoparticles after the film formation and

oxidation steps. There may be several fundamental problems that affect the polymer particle interactions in solution phase and causing these disordered aggregates of nanoparticles. These problems can be aroused from the competing interactions between solvent, polymer chains and metal particles. Another reason can involve polymer conformational entropy when the particles are adhered to the chains.[81] The conformation of the polymer chains adhered to the particles influences the controlled alignment of the particles. For example, Hashimoto et al. showed that depending on the molecular weight of the P2VP-b-PI copolymer the Pd nanoparticles can be aligned in the middle of P2VP lamellae, near the middle and also along the interfaces with the PI lamellae.[75,81,82] The molecular weight and composition of P2VP-b-PI block copolymers affect configurations of the copolymer chains adsorbed on the particle.

On the other hand, thin film doping does not involve these problems because doping occurs on the microphase separated structure. We observed the lamellar structure of an undoped poly(norbornene methanol)-b-poly(norbornene dicarboxylic acid) diblock copolymer by TEM and examined the dispersion of Fe_2O_3 nanoparticles within this polymer matrix when solution phase and thin film doping techniques were used. The comparison of the copolymer morphology before and after doping reveals the influence of the copolymer structure on the resulting nanoparticle dispersion within the polymer matrix. It was shown that the block copolymer guided the confinement of iron oxide nanoparticles within one of the microphase separated lamellae when the thin film doping technique was employed.

Chapter 6

Conclusions

The synthesis of novel poly(norbornene)-b-poly(deuterated norbornene dicarboxylic acid) diblock copolymers by ring-opening metathesis polymerization has been reported in this dissertation. The microstructures obtained by changing the volume fraction of one of the blocks was investigated by transmission electron microscopy and spherical, cylindrical and lamellar morphologies were observed. The microphase separated structures with different domain spacings were studied using small-angle neutron and X-ray scattering. These morphologies were used as templates for the synthesis of iron oxide nanoparticles. The distribution of Fe_2O_3 nanoparticles was controlled within NOR-b-NORCOOH copolymers when these polymer systems were doped with low amounts of iron (4 wt%), forming isolated spherical particles in the polymer template. Undoped copolymers with cylindrical and lamellar morphologies were doped with the stoichiometric amount of iron salts through a solution doping method. It was observed that at high iron concentrations (at 6 wt% and higher), iron oxide particles were not templated within the microdomains of the copolymers and formed interconnected structures. Small-angle X-ray and neutron scattering mea-

surements of iron oxide doped copolymers confirmed the non-uniform distribution of nanoparticles and indicated the influence of particles in the polymer microphase separation for samples with high Fe concentrations. The amount of nanoparticles and their dispersion influenced the interparticle interactions and the resultant magnetic behavior. As the Fe concentration increased in these samples, a change in the blocking temperatures was observed which indicated increased particle interactions for the samples displaying an interconnected morphology. All iron oxide doped samples exhibited superparamagnetic behavior at 300K and became ferrimagnetic at 10K.

It was found that solution doping was effective in templating iron oxide nanoparticles at low Fe concentration. The influence of high iron amounts (when added in solution) on the resultant polymer microphase separation has been confirmed by another experimental study of Hashimoto et al. using transmission electron microscopy. High inorganic particle content can suppress the microphase separated morphology and leads to interconnected aggregates. In future studies, phase diagrams of diblock copolymer with inorganic particles can be simulated and studied theoretically in order to understand the effect of particle size and volume fraction on the block copolymer morphologies. Polymer-solvent, polymer-particle and metal ion-solvent interactions should be considered in the theoretical calculations.

In the second part of the thesis, the synthesis of poly(norbornene methanol)-b-poly(norbornene dicarboxylic acid) diblock copolymers was reported. The lamellar structure of an undoped poly(norbornene methanol)-b-poly(norbornene dicarboxylic acid) diblock copolymer was observed by TEM and the dispersion of Fe_2O_3 nanopar-

ticles within this polymer matrix was investigated when solution phase and thin film doping techniques were used. It was shown that the block copolymer guided the confinement of iron oxide nanoparticles within one of the microphase separated lamellae when the thin film doping technique was employed. Iron oxide nanoparticles formed after solution doping were superparamagnetic. This nanocomposite presented a magnetization value of 73emu/γ-Fe_2O_3 at 5K which is very close to the saturation magnetization of bulk γ-Fe_2O_3 (M_s=82emu/g at 5K).

The synthesized iron oxide doped norbornene block copolymers can be used as magnetic refrigerants due to their high magnetization values at low temperatures. The current magnetization of the superparamagnetic nanoparticles can be also used for the drug delivery systems and magnetic resonance imaging.

Norbornene based diblock copolymers that were characterized in this study present ordered microstructures and they are potentially good candidates for stabilizing inorganic nanoparticles when thin film doping method was used. In future studies, the copolymer thin films can be formed by spin casting and they can be thermally annealed to achieve equilibrium structures. These preformed thin films and microphase separated equilibrium structures can be loaded with the particles by submersion into metal salt solutions. Using this metal loading method, templating of nanoparticles within all microstuctures of undoped copolymer can be studied in future experiments.

The copolymer of lamellar morphology that is doped with Fe_2O_3 particles using the above mentioned thin film doping can be studied in neutron reflectometry measurements. From the neutron reflectometry experiments, the period of the lamellar

structure and the position of the nanoparticles in the NORCOOH layers can be determined. The arrangement of the particles either in the interfaces of the two blocks or in the middle of the NORCOOH domain gives us information on the coordination of the iron oxide particles in the copolymer matrix.

In addition, the copolymer can be loaded with very low iron salt concentration in solution phase (0.005 M). In this case, attractive interactions between Fe ions will be neglected and the microphase separation probably will not be influenced by the presence of the nanoparticles. The interaction between carboxylic acid groups and the Fe ions will be dominant and the particles can be templated at low metal salt concentrations. Templated nanoparticles within ordered microstructures can lead to non-interacting behavior of the particles. This behavior may result in aligned magnetic anisotropy and higher magnetization values at room temperatures which can be practically used for high-density data storage media and electromagnetic systems. The particle size can be increased by overdoping the copolymers but the preformed structures will be destroyed. The self-assembled ordered copolymer structures should be maintained after particle incorporation and the effect of the ordered particles on the resultant properties can be studied in future experiments.

BIBLIOGRAPHY

[1] Kodama M. H., "Magnetic Nanoparticles", J.Magn.Magn.Mater. 200, 359-372 (1999).

[2] Predoi D., Kuncser V., Tronc E., Nogues M., Russo U., Principi G., Filoti G., "Magnetic relaxation phenomena and interparticle interactions in nanosized γ-Fe_2O_3 systems", J.Phys.:Condens.Matter 15, 1797-1811 (2003).

[3] Sohn B. H., Cohen R. E., "Processible optically transparent block copolymer films containing superparamagnetic iron oxide nanoclusters", Chem.Mater. 9, 264-269 (1997).

[4] Caro deD., Ely T. O., Mari A., Chaudret B., Snoeck E., Respaud M., Broto J-M., Fert A., "Synthesis, characterization, and magnetic studies of nonagglomerated zerovalent iron particles. Unexpected size dependence of the structure", Chem.Mater. 8, 1987-1991 (1996).

[5] Cheng J. Y., Ross C. A., Chan V. Z. -H., Thomas E. L., Lammertink R. G. B., Vancso G. J., "Formation of a Cobalt Magnetic Dot Array via Block Copolymer Lithography", Adv.Mater. 13, 1174-1178 (2001).

[6] Park M., Harrison C., Chaikin P. M., Register R. A., Adamson D. H., "Block copolymer lithography: Periodic arrays of $10^1 1$ holes in 1 square centimeter", Science 276, 1401-1404 (1997).

[7] Ciebien J. F., Cohen R. E., Duran A., "Catalytic properties of palladium nanoclusters synthesized within diblock copolymer films: hydrogenation of ethylene and propylene", Supramol.Sci. 5, 31-39 (1998).

[8] Chan Y. N. C., Craig G. S. W., Schrock R. R., Cohen R. E., "Synthesis of palladium and platinum nanoclusters within microphase separated diblock copolymers", Chem.Mater. 4, 885-894 (1992).

[9] Ciebien J. F., Clay R. T.,Sohn B. H., Cohen R. E., "Brief review of metal nanoclusters in block copolymer films", New J.Chem. 7, 685-691 (1998).

[10] Cummins C. C., Schrock R. R., Cohen R. E., "Synthesis of ZnS and CdS within ROMP block copolymer microdomains", Chem.Mater. 4, 27-30 (1992).

[11] Sankaran V., Yue J., Cohen R. E., Schrock R. R., Silbey R. J., "Synthesis of zinc sulfide clusters and zinc particles within microphase separated domains of organometallic block copolymers", Chem.Mater. 5, 1133-1142 (1993).

[12] Sankaran V., Cohen R. E., Cummins C. C., Schrock R. R., "Morphology of Diblock Copolymers of Norbornene and Organometallic Derivatives of Norbornene", Macromolecules 24, 6664-6669 (1991).

[13] Klabunde K. J., Habdas J., Cardenas-Trivino G., "Colloidal metal particles dispersed in monomeric and polymeric styrene and methyl methacrylate", Chem.Mater. 1, 481-483 (1989).

[14] Watkins J. J., McCarthy T. J., "Polymer/metal nanocomposite synthesis in supercritical CO_2", Chem.Mater. 7, 1991-1994 (1995).

[15] Clay R. T., Cohen R. E., "Synthesis of metal nanoclusters within microphase separated diblock copolymers: sodium carboxylate vs carboxylic acid functionalization", Supramol.Sci. 5, 41- (1998).

[16] Clay R. T., Cohen R. E., "Synthesis of metal nanoclusters within microphase-separated diblock copolymers: a 'universal approach", Supramol. Sci. 2, 183-191 (1995).

[17] Antonietti M., Forster S., Hrtmann J., Oestreich S., "Novel amphiphilic block copolymers by polymer reactions and their use for solubilization of metal salts and metal colloids", Macromolecules 29, 3800-3806 (1996).

[18] Ahmed S. R., Kofinas P., "Controlled room temperature synthesis of $CoFe_2O_4$ nanoparticles through a block copolymer route", Macromolecules 35, 3338-3341 (2002).

[19] Sohn B.H., Cohen R. E., Papaefthymiou G. C., "Magnetic properties of iron oxide nanoclusters within microdomains of block copolymers", Journ.Magn.Magn.Mater. 182, 216-224 (1998).

[20] Morkved T. L., Wiltzius P., Jaeger H. M., Grier D. G., Witten T. A., "Mesoscopic self-assembly of gold-islands on diblock copolymer films", Appl.Phys.Lett. 64, 422-424 (1994).

[21] Yue J., Cohen R. E., "Nanoreactors for inorganic cluster synthesis", Supramol.Sci. 1, 117-122 (1994).

[22] Kane R. S., Cohen R. E., Silbey R., "Synthesis of PbS nanoclusters within block copolymer nanoreactors", Chem.Mater. 8, 1919-1924 (1996).

[23] Kane R. S., Cohen R. E., Silbey R., "Synthesis of doped ZnS nanoclusters within block copolymer nanoreactors", Chem.Mater. 11, 90-93 (1999).

[24] Hashimoto T., Harada M., Sakamoto N., "Incorporation of metal nanoparticles into block copolymer nanodomains via in-situ reduction of metal ions in microdomain space", Macromolecules 32, 6867-6870 (1999).

[25] Garcia C., Zhang Y., DiSalvo F., Wiesner U., "Mesoporous aluminosilicate materials with superparamagnetic γ-Fe_2O_3 particles embedded in the walls", Angew. Chem.Int.Ed. 42, 1526-1530 (2003).

[26] Simon P. F. W., Ulrich R., Spiess H. W., Wiesner U., "Block copolymer - ceramic hybrid materials from organically modified ceramic precursors", Chem. Mater. 13, 3464-3486 (2001).

[27] Abes J. I., Cohen R. E., Ross C. A., "Selective growth of cobalt nanoclusters in domains of block copolymer films", Chem.Mater. 15, 1125-1131 (2003).

[28] Sun S., Murray C. B., "Synthesis of monodisperse cobalt nanocrystals and their assembly into magnetic superlattices", J.Appl.Phys. 85, 4325-4330 (1999).

[29] Sun S., Murray C. B., Weller D., Folks L., Moser A., "Monodisperse FePt nanoparticles and ferromagnetic FePt nanocrystal superlattices", Science 287, 1989-1992 (2000).

[30] Richter H. J., "Recent advances in the recording physics of thin-film media", J.Phys.D:Appl.Phys. 32, R147-R168 (1999).

[31] Kodama R. H., Berkowitz A. E., "Atomic-scale magnetic modeling of oxide nanoparticles", Phys.Rev.B 59, 6321-6336 (1999).

[32] Morales M.P., Veintemillas-Verdaguer S., Montero M. I., Serna C. J., "Surface and internal spin canting in γ-Fe_2O_3 nanoparticles", Chem.Mater. 11, 3058-3064 (1999).

[33] Spatz P. J., Mossmer S., Hartmann C., Moller M., "Ordered deposition of inorganic clusters from micellar block copolymer films", Langmuir 16, 407-415 (2000).

[34] Selvan S. T., Hayakawa T., Nogami M., Moller M., "Block copolymer mediated synthesis of gold quantum dots and novel gold-polypyrrole nanocomposites", J. Phys. Chem. B 103, 7441-7448 (1999).

[35] Flory P. J., "Principles of polymer chemistry", Ithaca, Cornell University Press (1953).

[36] Bates F. S., "Polymer-polymer phase behavior", Science 251, 898-904 (1991).

[37] Leibler L., "Theory of microphase separation in block copolymers", Macromolecules 13, 1602-1617 (1980).

[38] Kent M. S., Saunders R. S., Nelson G. C., Small J. H., "Adsorbed monolayers based on functionalized diblock copolymers", Macromolecules 30, 3942-3945 (1997).

[39] Grubbs R. H., Chang S., "Recent advances in olefin metathesis and its application in organic synthesis", Tetrahedron 54, 4413-4450 (1998).

[40] Weck M., Schwab P., Grubbs R. H., "Synthesis of ABA triblock copolymers of norbornenes and 7−oxanorbornenes via living ring-opening metathesis polymerization using well-defined, bimetallic rythenium catalysts", Macromolecules 29, 1789-1793 (1996).

[41] Schwab P., Grubbs R. H., Ziller J. W., "Synthesis and applications of $RuCl_2(=CHR^1)(PR_3)_2$: The influence of the alkylidene moiety on metathesis activity", J.Am.Chem.Soc. 118, 100-110 (1996).

[42] Lynn D. M., Kanaoka S., Grubbs R.H., "Living Ring-Opening Metathesis polymerization in aqueous media catalyzed by well-defined Ruthenium carbene complexes", J.Am.Chem.Soc. 118, 784-790 (1996).

[43] Demonceau A., Stumpf A. W., Saive E., Noels A. F., "Novel Ruthenium-Based catalyst systems for the ring-opening metathesis polymerization of low-strain cyclic olefins", Macromolecules 30, 3127-3136 (1997).

[44] Ivin K. J., Mol J. C., "Olefin Metathesis and Metathesis Polymerization", Academic Press, London, 1997.

[45] Pelecky-Leslie D. L., Rieke R. D., "Magnetic properties of nanostructured materials", Chem. Mater. 8, 1770-1783 (1996).

[46] Xavier B., Labarta A., "Finite-size effects in fine particles: magnetic and transport properties", J.Phys.D:Appl.Phys. 35, R15-R42 (2002).

[47] Morup S., "Superparamagnetism and spin glass ordering in magnetic nanocomposites", Europhys.Lett. 28, 671-676 (1994).

[48] Morup S., Tronc E., "Superparamagnetic relaxation of weakly interacting particles", Phys.Rev.Lett. 72, 3278-3281 (1994).

[49] Shtrikman S., Wohlfarth E. P., "The theory of the Vogel-Fulcher law of spin glasses", Phys.Lett.A 85, 467-470 (1981).

[50] Fiorani D., Dormann J. L., Cherkaoui R., Tronc E., Lucari F., D'Orazio F., Spinu L., Nogues M., Garcia A., Testa A. M., "Collective magnetic state in nanoparticles systems", Journ.Magn.Magn.Mater. 196-197, 143-147 (1999).

[51] Dormann J. L., Fiorani D., Cherkaoui R., Tronc E., Lucari F., D'Orazio F., Spinu L., Nogues M., Kachkachi H., Jolivet J. P., "From pure superparamgnetism to glass collective state in γ-Fe_2O_3 nanoparticle assemblies", Journ.Magn.Magn.Mater. 203, 23-27 (1999).

[52] Coey J. M. D., "Noncollinear spin arrangement in ultrafine ferrimagnetic crystallites", Phys.Rev.Lett. 27, 1140-1142 (1971).

[53] Kodama R. H., Berkowitz A. E., McNiff E. J., Foner S., "Surface spin disorder in ferrite nanoparticles (invited)", J.Appl.Phys. 81, 5552-557 (1997).

[54] Kodama R. H., Berkowitz A. E., McNiff E. J., Foner S., "Surface spin disorder in $NiFe_2O_4$ nanoparticles", Phys.Rev.Lett. 77, 394-397 (1996).

[55] Linderoth S., Hendriksen P. V., Bodker F., Wells S., Davies K., Charles S. W., "On spin-canting in maghemite particles", J.Appl.Phys. 75, 6583-6585 (1994).

[56] Del Bianco L., Hernando A., Multigner M., Prados C., Sanchez-Lopez J. C., Fernandez A., Conde C. F., Conde A., "Evidence of spin disorder at the surface-core interface of oxygen passivated Fe nanoparticles", J.Appl.Phys. 84, 2189-2192 (1998).

[57] Martinez B., Obradors X., Balcells L., Rouanet A., Monty C., "Low temperature surface spin-glass transition in γ-Fe_2O_3 nanoparticles", Phys.Rev.Lett. 80, 181-184 (1998).

[58] Bacon G. E., "Neutron Diffraction", second edition, Oxford at the Clarendon Press (1962).

[59] Bellouard C., Mirebeau I., Hennion M., "Magnetic correlations of fine ferromagnetic particles studied by small-angle neutron scattering", Phys.Rev.B 53, 5570-5578 (1996).

[60] Clay R. T., Cohen R. E., "Synthesis of Cu and CuO nanoclusters within microphase-separated diblock copolymers", New J.Chem. 7, 745-748 (1998).

[61] Boontongkong Y., Cohen R. E, Rubner M. F., "Selective Electroless Copper Deposition within Block Copolymer Microdomains", Chem.Mater. 12, 1628-1633 (2000).

[62] Chan Y. N. C, Schrock R. R., Cohen R. E., "Synthesis of silver and gold nanoclusters within microphase-separated diblock copolymers", Chem.Mater. 4, 24-27 (1992).

[63] Ahmed S. R., Ogale S. B., Kofinas P., "Magnetic Properties and Morphology of Block Copolymer Templated Ferrrimagnetic CoFe2O4 Nanoparticles", IEEE Trans Magn 39, 2198-2200 (2003).

[64] Saunders R. S., Cohen R. E., Schrock R. R., "Synthesis and Characterization of diblock copolymer containing self-assambled polyacetylene structures", Macromolecules 24, 5599-5605 (1991).

[65] National Institute of Standards and Technology Center for Neutron Research, NG3 and NG7 30-meter SANS instr uments data acquisition manual, June 2002.

[66] McIntyre N. S., Zetaruk D. G., "X-ray photoelectron spectroscopic studies of iron oxides", Anal.Chem. 49, 1521-1529 (1977).

[67] Watanabe T., Ooba N., Hida Y., Hikita M., "Influence of humidity on refractive index of polymers for opt ical waveguide and its temperature dependence", App.Phys.Lett. 72, 1533-1535 (1998).

[68] Roe R. J., "Methods of x-ray and neutron scattering in polymer science", Oxford University Press (2000).

[69] Seehra M. S., Babu V. S., Manivannan A., Lynn J. W., "Neutron scattering and magnetic studies of ferrihydrite nanoparticles", Phys.Rev.B 61, 3513-3518 (2000).

[70] Spizzo F., Angeli E., Bisero D., Da Re A., Ronconi F., Vavassori P, Bergenti I, Deriu A, Hoell A., "Small-angle neutron scattering measurements with polarised neutrons on Fe-Ag magnetic granular systems", J.Appl.Cryst. 36, 826-828 (2003).

[71] Dormann J. L., Bessais L., Fiorani D., J.Phys.C: Solid State Phys. 21, 2015-2034 (1988).

[72] Dormann J. L., Spinu L., Tronc E., Jolivet J. P., Lucari F., D'Orazio F., Fiorani D., "Effect of interparticle interactions on the dynamical properties of Fe_2O_3 nanoparticles", Journ.Magn.Magn.Mater. 183, L255-L260 (1998).

[73] Lin Y., Boker A., He J., Sill K., Xiang H., Abetz C., Li X., Wang J., Emrick T., Long S., Wang Q., Balazs A., Russell T. P., "Self-directed self-assembly of nanoparticle/copolymer mixtures", Nature 434, 55-59 (2005).

[74] Akcora P., Zhang X., Varughese B., Briber R. M., Kofinas P., "Structural and magnetic characterization of norbornene-deuterated norbornene dicarboxylic acid diblock copolymers doped with iron oxide nanoparticles", Polymer 2005, in press.

[75] Ribbe A. E., Okumura A., Matsuhige K., Hashimoto T., "Element spectroscopic imaging of poly(2-vinylpyridine)-block-polyisoprene microdomains containing palladium nanoparticles", Macromolecules 34, 8239-8245 (2001).

[76] Balazs A. C., "Interactions of nanoscopic particles with phase-separating polymeric mixtures", Curr.Op.Coll.Int.Sci. 4, 443-448 (2000).

[77] Balazs A. C., Ginzburg V.V., Qiu F., Peng G.,Jasnow D., "Multi-scale model for binary mixtures containing nanoscopic particles", J. Phys. Chem. 104, 3411-3422 (2000).

[78] Huh J., Ginzburg V. V., Balazs A. C., "Thermodynamic behavior of particle/diblock copolymer mixtures: simulation and theory", Macromolecules 33, 8085-8096 (2000).

[79] Royappa A. T., Saunders R. S., Rubner M. F., Cohen R. E., "Langmuir-Blodgett Films of Conducting Diblock Copolymers", Langmuir 14, 6207-6214 (1998).

[80] Gratt J., Cohen R. E., "Synthesis of block copolymers containing pendant carbazole groups via living ring-opening metathesis polymerization", Macromolecules 30, 3137-3140 (1997).

[81] Hashimoto T., Okumura A., Tanabe D., "Visualization of isolated poly(2-vinylpyridine)-block-polyisoprene chains adhered to isolated palladium nanoparticles", Macromolecules 36, 7324-7330 (2003).

[82] Tsutsumi K., Funaki Y., Hirokawa Y., Hashimoto T., "Selective incorporation of palladium nanoparticles into microphase-separated domains of poly(2-vinylpyridine)-block-polyisoprene", Langmuir 15, 5200-5203 (1999).